environments

MDPI

Article

Assessing the Spatial Distribution and Quality of Groundwater Resources in the Dehradun Region of India

Ankit Bisht [1], Tamás Mester [1,*] and Dániel Balla [2]

[1] Department of Landscape Protection and Environmental Geography, University of Debrecen, H-4032 Debrecen, Hungary; ankit.bisht@science.unideb.hu
[2] Department of Data Science and Visualization, Faculty of Informatics, University of Debrecen, H-4028 Debrecen, Hungary; balla.daniel@inf.unideb.hu
* Correspondence: mester.tamas@science.unideb.hu

Abstract

This study examines the spatiotemporal variability in groundwater quality at five monitoring locations in Dehradun, Uttarakhand, India, from 2021 to 2025, based on 40 site-period observations covering 33 physicochemical, ionic, trace metal and pesticide parameters. Most parameters complied with BIS IS:10500 (2012) standards, with total dissolved solids and total hardness well within limits. Sulphate peaked at 260.5 mg/L at a landfill site in 2023, and iron reached 13.2 mg/L at an industrial site, while arsenic, mercury, lead, cadmium and four organochlorine pesticides stayed below detection. Trend analysis showed significant declines in TDS, sulphate and sodium and a significant rise in pH, indicating improving water quality since 2021, although a sensitivity check restricted to 2022–2024 showed the pH and sulphate trends were driven mainly by recovery from the 2021 baseline rather than a continuing multi-year trend. A major-ion Water Quality Index classified groundwater as excellent to good at all sites, while a Heavy Metal Pollution Index, driven mainly by chromium in 2021 and nickel in post-monsoon 2022 rather than by iron, exceeded the critical value of 100 in 11 of 40 site-period observations. Piper trilinear analysis identified a predominantly Ca-HCO_3 hydrochemical facies at the individual-sample level, with a minority of samples showing mixed or sulphate-leaning compositions. A human health risk assessment based on copper, zinc, nickel and chromium showed hazard indices above the safety threshold at all sites in 2021, largely due to a conservative assumption that all measured chromium was present as the more toxic Cr(VI) form, with substantially lower hazard-index values from 2023 onward under the primary zero-substitution convention for below-detection-limit metals. A sensitivity check substituting half of the laboratory's documented detection limits for non-detect readings in these metals placed all 40 site-periods in the critical HPI band and raised the child hazard index above 1 in every 2022–2025 round outside post-monsoon 2022, so the post-2021 improvement is assumption-dependent. Conventional irrigation indices indicated low sodium and salinity hazards, although the very low electrical conductivity implies potential infiltration constraints under FAO EC-SAR guidance.

Keywords: groundwater quality; Dehradun; temporal analysis; BIS standards; sulphate; iron; trend analysis; Uttarakhand; physicochemical parameters

Check for updates

Academic Editor: Melida Gutierrez

Received: 24 September 2026
Revised: 13 October 2026
Accepted: 14 October 2026
Published: 16 October 2026

Copyright: © 2026 by the authors. Licensee MDPI, Basel, Switzerland. This article is an open access article distributed under the terms and conditions of the Creative Commons Attribution (CC BY) license.

1. Introduction

Although the total percentage of water in Earth's crust remains relatively constant [1–3], its accessible freshwater resources, quality, and distribution are increasingly compromised by anthropogenic exploitation exceeding natural recharge rates [4,5].

Groundwater is the predominant source of freshwater for domestic, commercial, and agricultural uses worldwide, accounting for a substantial share of irrigation water. In India, groundwater extraction is particularly intensive, surpassing the combined abstraction of the United States and China, largely driven by agricultural demands. Over-extraction has led to declining water tables, drying of natural springs, exhaustion of artesian wells, and aquifer depletion in many regions [6]. Concomitant contamination exacerbates these issues, posing risks to human health and ecosystems [7–9].

Key drivers of groundwater depletion and contamination include overexploitation for irrigation, with almost 89% of groundwater in India used for this purpose [10], domestic supply, and water-intensive industries such as paper manufacturing, food processing, bottled water production, and tanneries [11–13]. Additional inputs come from untreated or poorly managed domestic sewage, agricultural runoff rich in nitrates and phosphates that promotes eutrophication in surface water bodies, and leachate from municipal solid waste (MSW) landfills, which can introduce heavy metals such as cadmium, mercury, arsenic, chromium and lead, along with pesticides and microbial pathogens [1,14,15]. Heavy metals are of particular concern because of their persistence, bioaccumulation, and carcinogenic potential [16,17]. The ageing underground pipeline network adds a further risk to public health, since it is poorly maintained and sections are sometimes corroded or broken [18].

In India, groundwater supplies approximately 45% of domestic water demand [19]. Rapid urbanisation and industrialisation in regions like Dehradun (the capital of Uttarakhand, located in the Doon Valley) intensify pressures. The valley is underlain by Quaternary alluvial deposits, rendering the shallow aquifers highly vulnerable to surface contamination from pharmaceutical manufacturing, MSW disposal, agricultural runoff, and inadequate sewage systems [20,21].

Despite this regulatory monitoring framework, published hydrogeochemical research on the Doon Valley remains comparatively fragmented with respect to temporal depth and source-specific comparison. Dudeja et al. [20] characterised the ionic composition of 76 groundwater sources across the wider valley and established a Ca-Mg-HCO_3 hydrochemical facies, but relied on a single spatio-seasonal sampling round without repeated observations over multiple years. Pundir et al. [18] applied multivariate statistics, a weighted arithmetic Water Quality Index (WQI) and Piper diagrams across the valley and reported that 96% of sources were of excellent to good quality, again from a single monitoring campaign that did not distinguish among specific anthropogenic source types. Nayak et al. [21] focused specifically on the Selaqui industrial belt and quantified a Heavy Metal Pollution Index, identifying iron, zinc and copper as the dominant contaminants with HPI values in the high but sub-critical range, an assessment similarly restricted to a single sampling period and without a landfill-influenced comparison site. Kamboj et al. [11] examined nitrate and fluoride health risk in the same industrial belt but did not extend the parameter suite to trace metals or hydrochemical facies. At a larger scale, Pandey et al. [22] integrated WQI and hydrochemical analysis across 338 wells in three Western Himalayan states between 2019 and 2022, offering a useful regional baseline but necessarily at a district-level resolution that cannot resolve differences between specific industrial and waste-disposal pressure types within a single peri-urban area. None of these studies combined repeated, multi-year monitoring with a paired comparison between industrial sites and MSW-associated pressure zones at the level of individual wells, nor did any integrate a major-ion Water

Quality Index with a complementary Heavy Metal Pollution Index and Piper-based facies determination within the same analysis.

The present study addresses this combination of gaps by synthesising eight rounds of secondary monitoring data (2021 to 2025) from five wells representing two contrasting anthropogenic pressure types in the Selaqui-Sisambada area of Dehradun. The specific objectives are, first, to characterise the physicochemical, major ion and trace metal profiles of groundwater at the five selected sites; second, to identify statistically significant temporal trends in water-quality parameters between 2021 and 2025; third, to determine dominant hydrochemical processes and facies using correlation analysis, principal component analysis and a Piper trilinear diagram; and fourth, to quantify overall water-quality status using a major-ion Water Quality Index alongside a complementary Heavy Metal Pollution Index, in order to support evidence-based groundwater management in this peri-urban Himalayan foothill setting.

2. Materials and Methods

2.1. Study Area and Monitoring Locations

The study area encompasses two micro-zones within Dehradun district (30.32° N, 78.03° E; elevation ~640 m asl; Figure 1): (i) Selaqui, a planned industrial township approximately 18 km west of Dehradun city, home to pharmaceutical and precision manufacturing units; and (ii) a municipal solid waste (MSW) landfill area approximately 3 km southeast of the Selaqui cluster (site L4). A second, more distant MSW-associated monitoring location (L5, approximately 15 km from L4) is also included in the dataset; both site coordinates have been confirmed against field records. The geology consists predominantly of Himalayan foreland alluvium with gravel–sand–silt sequences, providing high permeability and recharge from the Song River catchment.

Five monitoring sites were designated:

- L1—Handpump, Pharma City (near Rusan Pharma), Selaqui
- L2—Handpump, Old Police Station, Industrial Area-1, Selaqui
- L3—Handpump, Honeywell Pvt. Ltd., Industrial Area-2, Selaqui
- L4—MSW Landfill Site, Sisambada, North Side
- L5—MSW Landfill Site, Sisambada, South Side
- L1, L2, L3—Together fall under the category of Industrial Sites in Selaqui
- L4, L5, together fall under the category of Municipal Solid Waste Management Sites.

These five points were selected to represent the principal anthropogenic pressures identified in the study area, industrial and pharmaceutical effluent at the Selaqui cluster (L1–L3) and municipal solid waste leachate at the MSW-associated sites (L4–L5), rather than to provide dense areal coverage of the wider Doon Valley aquifer. Consequently, the spatial findings reported in this study characterise these two specific pressure zones and should not be extrapolated to the aquifer as a whole without additional monitoring points.

2.2. Data Collection and Sampling

Secondary data were sourced from the Uttarakhand State Pollution Control Board (UPCB). Sampling was conducted at varying frequencies, annually in 2021, semi-annually from 2022 to 2024, and once in 2025, yielding eight monitoring periods (pre-monsoon and post-monsoon where applicable), and reportedly followed BIS IS:3025 (Part 1) procedures for groundwater sampling and preservation. Field parameters recorded at each visit also included temperature, colour and odour. Parameters retained for quantitative analysis included physicochemical attributes (pH, TDS, EC), major ions—total hardness, calcium hardness and magnesium hardness, all expressed as $CaCO_3$ equivalents (mg/L as $CaCO_3$); sodium, potassium, chloride, sulphate, fluoride and nitrate-nitrogen, expressed as the

elemental or ionic species; and total alkalinity, expressed as $CaCO_3$—and trace metals (As, Ni, Cu, Hg, Cr, Cd, Zn, Pb, Fe). The complete set of 33 parameters retained for analysis, with units and parameter groups, is provided in Supplementary Table S5, which also lists the analytical method (atomic absorption spectrophotometry (AAS) for the trace metals and general laboratory instrumentation for the remaining parameters) and the laboratory's Lowest Detection Limit for each parameter. As an internal data-quality check, electrical conductivity was cross-validated against total dissolved solids using the empirical EC/TDS ratio, which is expected to fall within approximately 1.2 to 2.2 for groundwater of this general composition. One value (site L2, October 2024) fell far outside this range and is flagged as a probable transcription error pending verification against the original laboratory record. It was therefore treated as missing in the trend and correlation analyses.

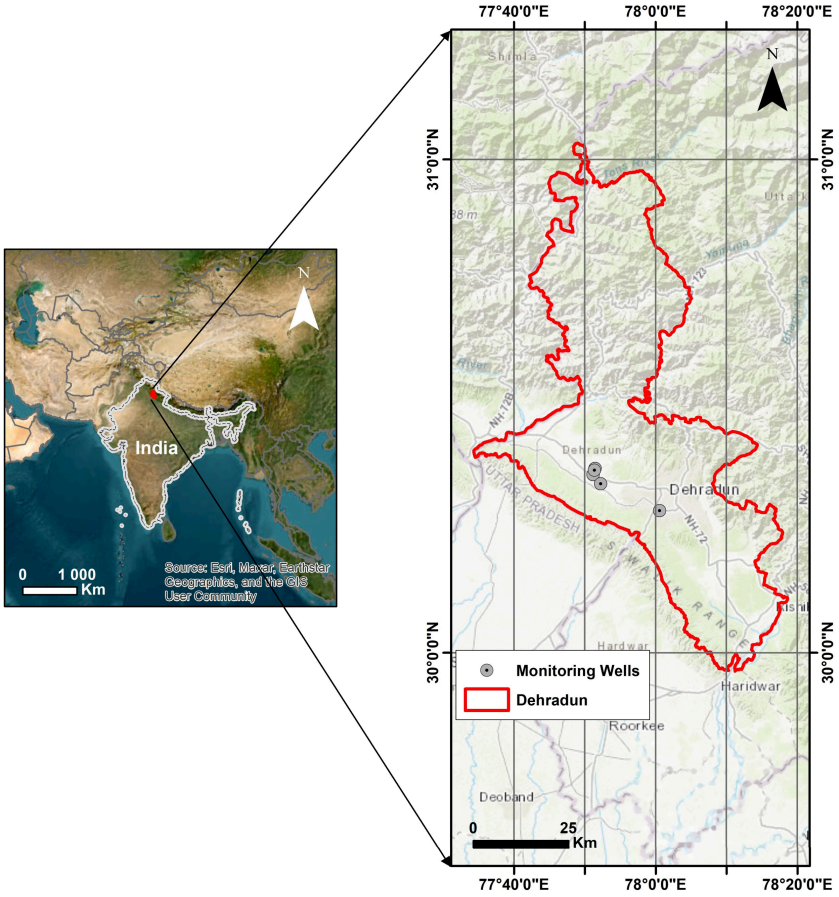


Figure 1. Location of study area and five groundwater monitoring sites (L1–L5) within the Selaqui industrial cluster and the Sisambada municipal solid waste landfill area. Basemap sources: Esri, HERE, Garmin, Intermap, increment P Corp., GEBCO, USGS, FAO, NPS, NRCAN, GeoBase, IGN, Kadaster NL, Ordnance Survey, Esri Japan, METI, Esri China (Hong Kong), © OpenStreetMap contributors and the GIS User Community.

2.3. Statistical Methods

All statistical analyses and indices were computed in Python (version 3.11; Python Software Foundation, Wilmington, DE, USA) using the pandas, NumPy, SciPy, scikit-learn and Matplotlib libraries, and the analysis script is available as described in the Data Availability Statement. QGIS (version 3.44.8-Solothurn; QGIS.org Association, Laax, Switzerland) was used for data preprocessing and mapping. Below-detection-limit (BDL/ND) values were assigned zero, a defensible zero-concentration assumption when no hazardous concentration of an analyte is detected in any site-related sample [23]. This condition was met for arsenic, mercury, lead, cadmium and all four screened organochlorine pesticides,

which were undetected in all 40 samples across the five-year monitoring period (2021–2025, across the eight sampling rounds), and the same convention was extended to the smaller number of non-detect readings among the remaining trace metals (copper, zinc, nickel, chromium) for consistency and comparability across the dataset. The source laboratory's own documented detection limits for these four metals are documented in its periodic monitoring reports (Supplementary Table S5: copper 0.03 mg/L, nickel 0.1 mg/L, chromium 0.06 mg/L, zinc 0.01 mg/L; Section 4.4); as a sensitivity check, the Heavy Metal Pollution Index and the human health hazard index were therefore also recalculated substituting half of each metal's own documented detection limit for every zero reading in that metal, and compared with the zero-substitution results reported below.

Descriptive statistics (mean, median, minimum, maximum and standard deviation) were computed for all 33 measured physicochemical, ionic, trace metal and organochlorine pesticide parameters. Pearson correlation coefficients with two-tailed significance testing were calculated among the 23 parameters with non-zero variance across the dataset. Trace metal pairs with detection frequencies below 35% (nickel, chromium, copper, zinc) yielded unstable pairwise correlation estimates based on as few as two co-occurring non-zero observations, at which sample size the Pearson coefficient is mathematically constrained to plus or minus one regardless of the underlying relationship; these specific metal-pair correlations, when restricted to that small paired non-zero subset, are not interpretable; Section 3.4 instead reports them recomputed on the full zero-substituted sample, where this degeneracy does not arise for all but the most severely non-detect-dominated pairs.

Kruskal–Wallis H-tests were applied to evaluate statistically significant differences among locations for each parameter. Ordinary least squares (OLS) linear regression was fitted to each parameter against a numeric monitoring-period index (0 to 7, corresponding to the eight sampling rounds) to quantify temporal trends, and 95% confidence intervals were computed using standard error propagation. Because sampling intervals were not perfectly uniform across the study period, the period-index regression was validated against an equivalent model using actual elapsed days since the first sampling round. The two approaches produced materially identical slope estimates, correlation coefficients and significance levels for every parameter tested (differences of 0.02 or less in r), confirming that the ordinal period index does not introduce meaningful bias despite the mixed annual and semi-annual sampling design. To assess whether pooling all five monitoring sites into a single trend model could inflate apparent significance through pseudoreplication, the OLS trend analysis was repeated with site included as a fixed effect. All previously significant trends (pH, TDS, EC, sulphate, sodium, total hardness, chloride) remained statistically significant after this adjustment, so the reported temporal trends do not appear to be an artefact of between-site differences in mean concentration alone. This adjustment, however, accounts only for differences in site-level means and does not by itself address temporal autocorrelation within a given well across repeated rounds, or dependence among the five sites sampled within the same campaign; it therefore reduces, rather than eliminates, the risk that the reported significance levels are optimistic, and the trend results below should be read with this caveat.

Water Quality Index (WQI) values were calculated for each site and monitoring period using a weighted arithmetic WQI adapted from Brown et al. [24], based on nine parameters with established BIS IS:10500 (2012) [25] acceptable limits (pH, TDS, total hardness, calcium, magnesium, chloride, sulphate, nitrate and fluoride). Unit weights were assigned as $w_i = K/S_i$, where S_i is the BIS acceptable limit for parameter i and K is a proportionality constant equal to the reciprocal of the sum of $1/S_i$ across the nine included parameters. Sub-indices were computed as $q_i = 100 \times (C_i - V_i)/(S_i - V_i)$, where V_i is the ideal value (zero for all parameters except pH, for which $V_i = 7.0$). Because pH has a two-sided BIS

acceptable range (6.5–8.5) that is not symmetric around the ideal value of 7.0 (a lower half-range of 0.5 versus an upper half-range of 1.5), its sub-index was instead computed piecewise: for pH below 7.0, the deviation was normalised to the lower BIS boundary distance ($qi = 100 \times |Ci - Vi|/0.5$), and for pH at or above 7.0, to the upper BIS boundary distance ($qi = 100 \times |Ci - Vi|/1.5$), so that both BIS boundaries (6.5 and 8.5) correspond to a sub-index of 100. WQI was obtained as the weighted mean of qi across all nine parameters. Because heavy metals are not represented in this major-ion WQI formulation and would dominate the index disproportionately if included given their comparatively strict regulatory limits, a complementary Heavy Metal Pollution Index (HPI) was calculated following Mohan et al. [26] for iron, copper, nickel, chromium and zinc, the trace metals with measurable concentrations in this dataset, using the same general weighting principle with a critical HPI threshold of 100.

Hydrochemical facies were assessed using a Piper trilinear diagram. Calcium and magnesium were reported in the source laboratory dataset as calcium hardness and magnesium hardness (mg/L as $CaCO_3$), confirmed by their exact additivity to the reported total hardness in every sample and by explicit column labelling in later monitoring rounds; these were converted to elemental Ca^{2+} and Mg^{2+} concentrations using Ca^{2+} (mg/L) = calcium hardness/2.497 and Mg^{2+} (mg/L) = magnesium hardness/4.118 before any further calculation, and this elemental basis was used throughout for the Piper diagram, the ionic charge balance, the Water Quality Index (Section 2.3) and the irrigation-suitability indices below. Major ion concentrations (Ca^{2+}, Mg^{2+}, $Na^+ + K^+$, HCO_3^-, Cl^-, SO_4^{2-}) were converted from mg/L to meq/L using standard equivalent weights, normalised to percentage of total cation or anion equivalents, and plotted on cation and anion ternary axes for every individual sample rather than site-period averages. A sample-level ionic charge-balance error (CBE% = $100 \times (\Sigma\text{cations} - \Sigma\text{anions})/(\Sigma\text{cations} + \Sigma\text{anions})$, where the cation and anion sums are expressed in meq/L) was computed for all 40 observations to assess internal consistency of the major-ion dataset. Principal component analysis (PCA) was performed on the 14 parameters with a detection frequency of at least 65% (pH, TDS, EC, hardness, calcium, magnesium, alkalinity, chloride, fluoride, sulphate, sodium, potassium, sodium adsorption ratio (SAR) and iron), standardised to zero mean and unit variance prior to extraction. The first two components were retained for interpretation based on the scree profile.

Non-carcinogenic human health risk from oral ingestion of copper, zinc, nickel and chromium was assessed following the standard USEPA [27,28] approach. Chronic daily intake (CDI, mg/kg-day) was calculated as $CDI = C \times IR \times EF \times ED/(BW \times AT)$, using default exposure factors: ingestion rate (IR) of 2.0 L/day for adults and 1.0 L/day for children, exposure frequency (EF) of 350 days/year, exposure duration (ED) of 30 years for adults and 6 years for children, body weight (BW) of 70 kg for adults and 15 kg for children, and averaging time (AT) equal to ED × 365 days. The hazard quotient (HQ) for each metal was obtained by dividing CDI by its oral chronic reference dose (RfD; USEPA IRIS: copper 0.04, zinc 0.3, nickel 0.02, chromium 9×10^{-4} mg/kg-day, the value updated by USEPA IRIS in August 2024 from the previously used value of 0.003 mg/kg-day), and the hazard index (HI) was calculated as the sum of the four hazard quotients, with HI greater than 1 indicating a potential non-carcinogenic health concern. This hazard index approach is a screening-level, non-carcinogenic assessment only. The 2024 IRIS update also introduced an oral cancer slope factor for hexavalent chromium (0.16 $(mg/kg\text{-}day)^{-1}$ for adults), so a screening-level incremental lifetime cancer risk (ILCR) was additionally estimated for the 2021 chromium detections as ILCR = LADD × CSF, using the same worst-case total-chromium-as-Cr(VI) assumption as above and a lifetime-averaged daily dose (LADD; using a 70-year averaging time rather than the exposure-duration-averaged AT used for

the hazard index above). Iron was excluded from this calculation because no USEPA oral reference dose has been established for it. Because trivalent and hexavalent chromium were not distinguished in the underlying dataset, total chromium was conservatively assumed to be entirely hexavalent (RfD = 9×10^{-4} mg/kg-day), the standard precautionary approach when speciation data are unavailable. A sensitivity check using the trivalent reference dose (1.5 mg/kg-day) is reported alongside the main result.

Irrigation water suitability was evaluated using five standard indices computed from major ion concentrations in meq/L, in addition to SAR, already reported in the source dataset and defined in Section 2.3: Kelly's ratio (KR = Na/(Ca + Mg); suitable below 1; Kelly [29]), magnesium hazard (MH = 100 × Mg/(Ca + Mg); suitability threshold 50%), the permeability index of Doneen (PI = 100 × (Na + sqrt(HCO_3))/(Ca + Mg + Na); Class I > 75% excellent, Class II 25–75% good, Class III < 25% unsuitable; Doneen [30]), percent sodium (%Na = 100 × (Na + K)/(Ca + Mg + Na + K); threshold 60%), and residual sodium carbonate (RSC = HCO3 − (Ca + Mg); safe below 1.25 meq/L). Samples were additionally classified for salinity and sodium (alkali) hazard using the United States Salinity Laboratory (USSL) diagram (electrical conductivity vs. SAR; USSL Staff [31]).

3. Results

3.1. Descriptive Statistics and Overall Water Quality

Descriptive statistics of the measured groundwater-quality parameters are summarised in Table 1. pH ranged from 5.68 to 7.36. All post-2021 values fell within the BIS acceptable range of 6.5–8.5, but all five 2021 baseline readings (5.68–6.17 across the five sites) fell below this range, indicating mild acidification at every site that recovered in subsequent rounds. TDS concentrations ranged from 35 to 199 mg/L, far below the BIS acceptable limit of 500 mg/L, pointing to low mineralisation typical of the recharge-dominated Doon Valley aquifer. Total hardness ranged from 68 to 220 mg/L, classifying groundwater as moderately soft to moderately hard [32], with calcium hardness (mean = 75.72 mg/L as $CaCO_3$) and magnesium hardness (mean = 22.90 mg/L as $CaCO_3$)—reported here, as in Table 1, on a $CaCO_3$-equivalent rather than elemental basis—the dominant contributors to total hardness.

Sulphate concentrations showed the widest variability of any parameter (range 0–260.52 mg/L, CV = 135%). The single highest value recorded in the entire dataset (260.52 mg/L) occurred at the L4 landfill site in pre-monsoon 2023 (although this value exceeds the total dissolved solids reported for the same sample and is one of the six flagged observations discussed in Section 4.4), while separately, early 2021 samples at the industrial sites L2 (240.26 mg/L) and L3 (213.17 mg/L) also approached or exceeded the BIS limit of 200 mg/L. Iron was also notably elevated in the early sampling periods, reaching 13.23 mg/L at L2 (2022-S1) and 9.11 mg/L at L1 (2022-S2), both more than 30 times the BIS acceptable limit of 0.3 mg/L.

Arsenic, mercury, lead and cadmium stayed below their respective detection limits in all 40 samples throughout the study period, as did the four screened organochlorine pesticides (aldrin, hexachlorobenzene, alpha-endosulfan and beta-endosulfan). None of these priority pollutants was detected at any site or time. Fluoride (range 0–0.72 mg/L) stayed well within the BIS limit of 1.0 mg/L, chloride (mean = 15.18 mg/L) was far below the 250 mg/L permissible limit, and nitrate-N was negligible (mean = 0.01 mg N/L) against the BIS limit of 45 mg/L NO_3^- (about 10.2 mg N/L as nitrate-nitrogen).

Table 1. Descriptive statistics of the analysed groundwater-quality parameters. The electrical conductivity row includes one value (24 µS/cm, L2, October 2024) that is flagged as a probable transcription error and treated as missing in the trend and correlation analyses (Section 2.2). Excluding it, electrical conductivity has n = 39, a minimum of 78 µS/cm and a mean of 180.63 ± 64.69 µS/cm.

Parameter	*N*	Min	Max	Mean	SD	Skewness	Kurtosis	BDL/ND (%)
pH (–)	40	5.68	7.36	6.64	0.35	−0.80	0.79	0.0
TDS (mg/L)	40	35	199	112.70	44.79	0.32	−1.03	0.0
EC (µS/cm)	40	24	286	176.71	68.49	−0.11	−0.92	0.0
Total hardness (mg/L as $CaCO_3$)	40	68	220	98.62	29.95	2.46	7.32	0.0
Calcium hardness (mg/L as $CaCO_3$)	40	56	160	75.72	21.12	2.96	9.67	0.0
Magnesium hardness (mg/L as $CaCO_3$)	40	6	82	22.90	15.29	2.23	5.54	0.0
Alkalinity (mg/L as $CaCO_3$)	40	54	120	83.95	16.42	0.24	−0.64	0.0
Chloride (mg/L)	40	0	29	15.18	6.93	0.16	−0.64	2.5
Fluoride (mg/L)	40	0.00	0.72	0.32	0.14	0.40	1.46	5.0
Nitrate (mg/L as N)	40	0.00	0.10	0.01	0.03	2.80	6.64	87.5
Nitrite (mg/L)	40	0.00	0.13	0.03	0.04	1.13	−0.07	57.5
Sulphate (mg/L)	40	0.00	260.52	52.35	75.53	1.82	1.90	10.0
Phosphate (mg/L)	40	0.00	0.25	0.05	0.09	1.26	−0.19	72.5
Sodium (mg/L)	40	0.00	29.40	12.14	7.44	0.39	−0.05	2.5
Potassium (mg/L)	40	0.00	3.90	1.31	0.95	0.58	1.11	22.5
SAR (–)	40	0.23	1.22	0.58	0.26	0.88	−0.17	0.0
Copper (mg/L)	40	0.00	0.08	0.01	0.02	2.09	3.19	75.0
Iron (mg/L)	40	0.00	13.23	1.71	2.83	2.75	7.65	12.5
Zinc (mg/L)	40	0.00	2.17	0.16	0.39	4.08	19.42	65.0
Nickel (mg/L)	40	0.00	0.32	0.03	0.09	2.49	4.67	87.5
Chromium (mg/L)	40	0.00	0.33	0.04	0.10	2.40	4.02	87.5
COD (mg/L)	40	0.00	5.60	1.45	2.38	1.05	−0.93	72.5
TKN (mg/L)	40	0.00	8.21	1.52	2.74	1.38	0.19	75.0

3.2. Spatial Distribution of Water Quality Indicators

The Heavy Metal Pollution Index (Figure 2) and iron concentration class (Figure 3) were mapped for each site across the monitoring periods that bracket the pollution episode, confirming that the episode affected all five sites rather than a single location. At the 2021 baseline, every site fell in the critical HPI category, driven almost entirely by chromium. At the 2022 post-monsoon peak, every site again fell in the critical category, this time driven almost entirely by nickel rather than iron. By the 2023 pre-monsoon recovery, all five sites had returned to the low category, an improvement that persisted through the 2025 sampling round.

The iron classification map (Figure 3) shows that the episode did not peak at every site in the same season. Site L2 reached its highest iron class (greater than 6.0 mg/L) in the 2022 pre-monsoon round, while site L1 reached the same class six months later, in the 2022 post-monsoon round. Both values exceed the BIS acceptable limit of 0.3 mg/L by more than an order of magnitude. A map restricted to post-monsoon rounds alone would have missed the L2 pre-monsoon peak entirely, which is why a pre-monsoon panel was included alongside the post-monsoon one. By 2025 iron had declined to the acceptable or permissible class at every site.

Complementary maps of pH and sulphate (Figure 4) show the same recovery from a different angle. Measured pH rose from a 2021 range of 5.68 to 6.17 across the five sites, all of which were below the BIS lower acceptable limit of 6.5, to a 2025 range of 6.61 to 7.36, entirely within the acceptable band. Sulphate fell from a 2021 range of 39.4 to 240.3 mg/L, approaching or exceeding the BIS acceptable limit of 200 mg/L at three of the five sites, to a 2025 range of 8.8 to 19.5 mg/L at every site.

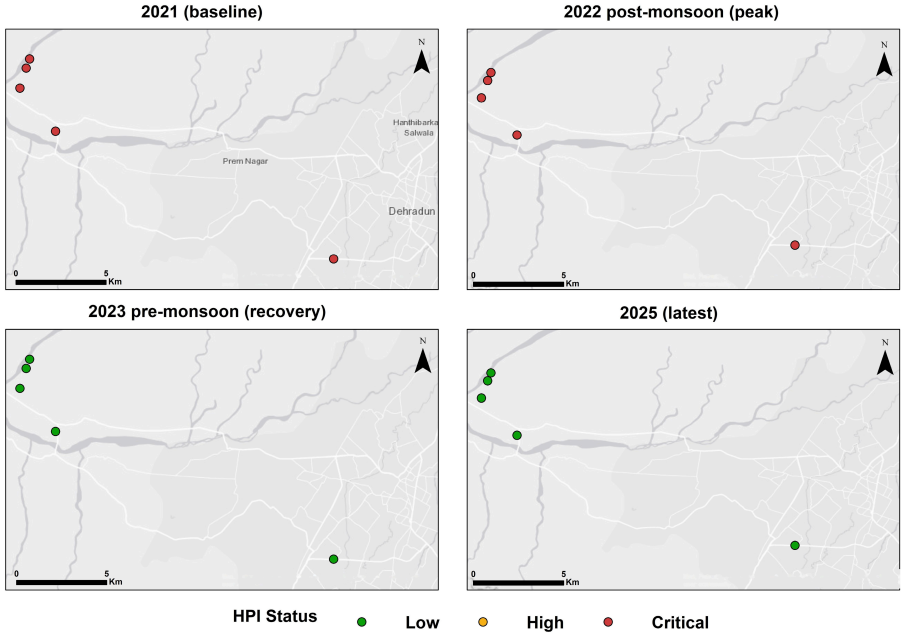


Figure 2. Spatial distribution of Heavy Metal Pollution Index (HPI) status at the five monitoring sites for four representative periods (2021 baseline, 2022 post-monsoon peak, 2023 pre-monsoon apparent recovery, 2025 latest). HPI status follows Mohan et al. [26]: low (HPI < 30), high (30–99), critical (HPI $\geq$ 100). These four periods are illustrative snapshots, not the complete temporal record; full site- and period-level HPI values for all eight monitoring rounds are provided in Table S3. Status is shown under the zero-substitution convention for non-detects. Under the detection-limit sensitivity check described in Section 3.6, all sites in the 2023 and 2025 panels would instead be classed as critical, so the apparent recovery should be read as provisional. Basemap sources: Esri, HERE, Garmin, © OpenStreetMap contributors and the GIS User Community.

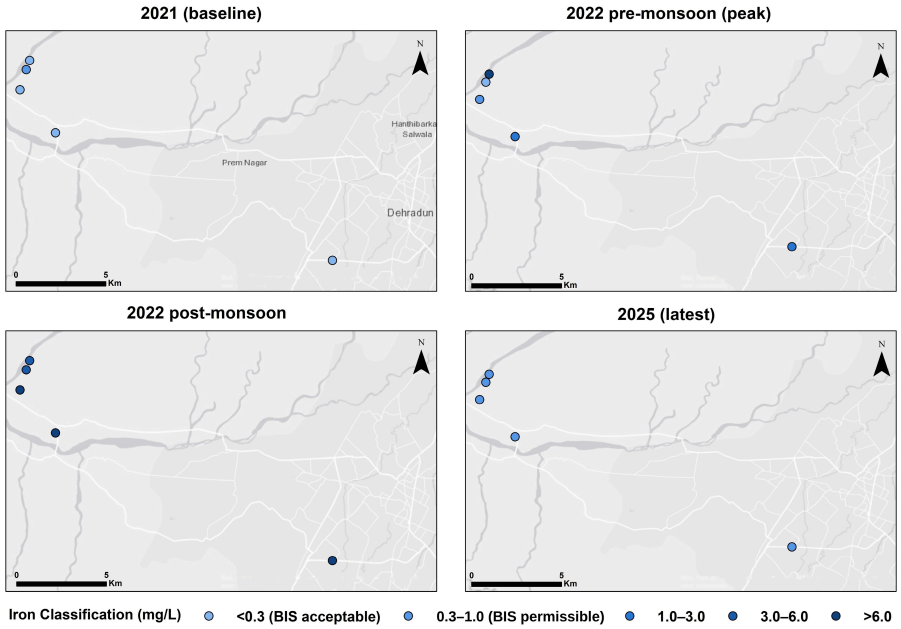


Figure 3. Spatial distribution of iron concentration class at the five monitoring sites for four periods spanning the 2022 trace-metal episode (2021 baseline, 2022 pre-monsoon, 2022 post-monsoon, 2025 latest). Classes follow the BIS IS:10500 (2012) acceptable (<0.3 mg/L) and permissible (0.3–1.0 mg/L) limits for iron, with three further classes above the permissible limit. Basemap sources: Esri, HERE, Garmin, © OpenStreetMap contributors and the GIS User Community.

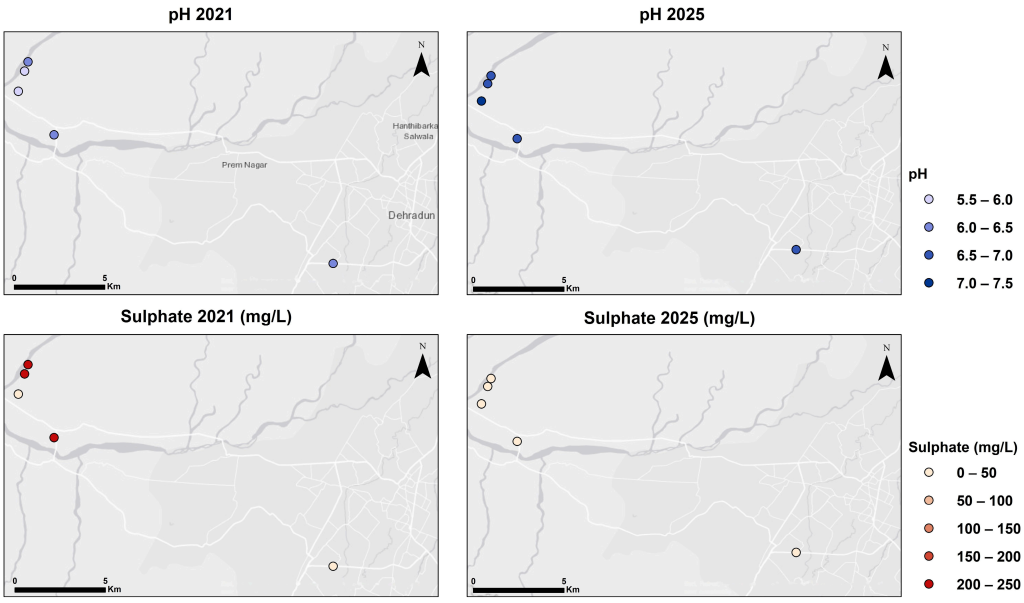


Figure 4. Spatial distribution of pH (**top row**) and sulphate (**bottom row**) at the five monitoring sites in 2021 and 2025. The 2021 sulphate values at L2, L3 and L4 exceed the total dissolved solids reported for the same samples and are flagged in Section 4.4. Basemap sources: Esri, HERE, Garmin, © OpenStreetMap contributors and the GIS User Community.

Spatially, the three industrial sites (L1 to L3) and the northern MSW landfill site (L4) cluster within a roughly 3 km radius northwest of Dehradun, while the southern MSW landfill site (L5) lies approximately 15 km to the southeast. Because the 2021–2022 trace-metal episode affected both the nearby industrial cluster and the more distant L5 site, it was not confined to one site type.

3.3. Temporal Trends

Linear regression analysis revealed several statistically significant temporal trends (Figures 5 and 6). pH increased significantly (slope = +0.076 units/period, r = 0.507, $p < 0.001$), rising from 5.68–6.17 in 2021 to 6.61–7.36 in 2025, possibly due to declining acid loading from industrial sources or natural alkalinity recovery. TDS declined significantly over the same period (slope = −13.10 mg/L/period, r = −0.678, $p < 0.001$), from 160–199 mg/L in 2021 to 54–75 mg/L in 2025, and EC followed an equivalent downward trajectory (slope = −20.32 µS/cm/period, r = −0.727, $p < 0.001$; computed with the L2, October 2024 anomaly excluded as missing, consistent with its treatment elsewhere in the trend and correlation analyses, Section 2.2). Together, these declines point to improved recharge dilution, reduced anthropogenic mineralisation inputs, or both.

Sulphate declined sharply (slope = −14.90 mg/L/period, r = −0.458, $p = 0.003$), from a 2021 peak of 240.26 mg/L at L2 to below 25 mg/L at most sites by 2025, a reduction that may reflect changes in source loading, recharge dilution, or both, although some of the earlier high values coincide with the sulphate data-quality concern discussed in Section 4.4. Sodium also declined significantly (slope = −2.61 mg/L/period, r = −0.813, $p < 0.001$), while chloride instead rose over the study period (slope = +1.02 mg/L/period, r = 0.342, $p = 0.031$). Total hardness showed a weaker decline that does not survive the multiple-testing correction applied below (slope = −4.29 mg/L/period, r = −0.333, $p = 0.036$), which, together with the calcium and magnesium trends, is more likely to reflect seasonal recharge variation than a directional anthropogenic change. Iron showed a declining slope (−0.30 mg/L/period) that did not reach statistical significance (r = −0.249, $p = 0.122$), owing to high variance (CV = 152%) from outlier observations in 2022. Beyond these seven parameters, eight further parameters with non-zero variance also showed a sta-

tistically significant pooled temporal trend that survives the multiple-testing correction described below: sodium adsorption ratio (slope = −0.085/period, r = −0.771, $p < 0.001$, tracking the sodium decline), total Kjeldahl nitrogen (slope = −0.851 mg/L/period, r = −0.720, $p < 0.001$), fluoride (slope = −0.037 mg/L/period, r = −0.605, $p < 0.001$), chromium (slope = −0.025 mg/L/period, r = −0.575, $p < 0.001$), nitrate-N (slope = −0.006 mg/L/period, r = −0.542, $p < 0.001$), magnesium (elemental concentration; slope = −0.731 mg/L/period, r = −0.457, $p = 0.003$, declining even though the parallel calcium trend is not significant), copper (slope = −0.004 mg/L/period, r = −0.421, $p = 0.007$) and nitrite-N (slope = −0.006 mg/L/period, r = −0.356, $p = 0.024$). The declining chromium trend is discussed further alongside the health-risk assessment in Section 4.1.

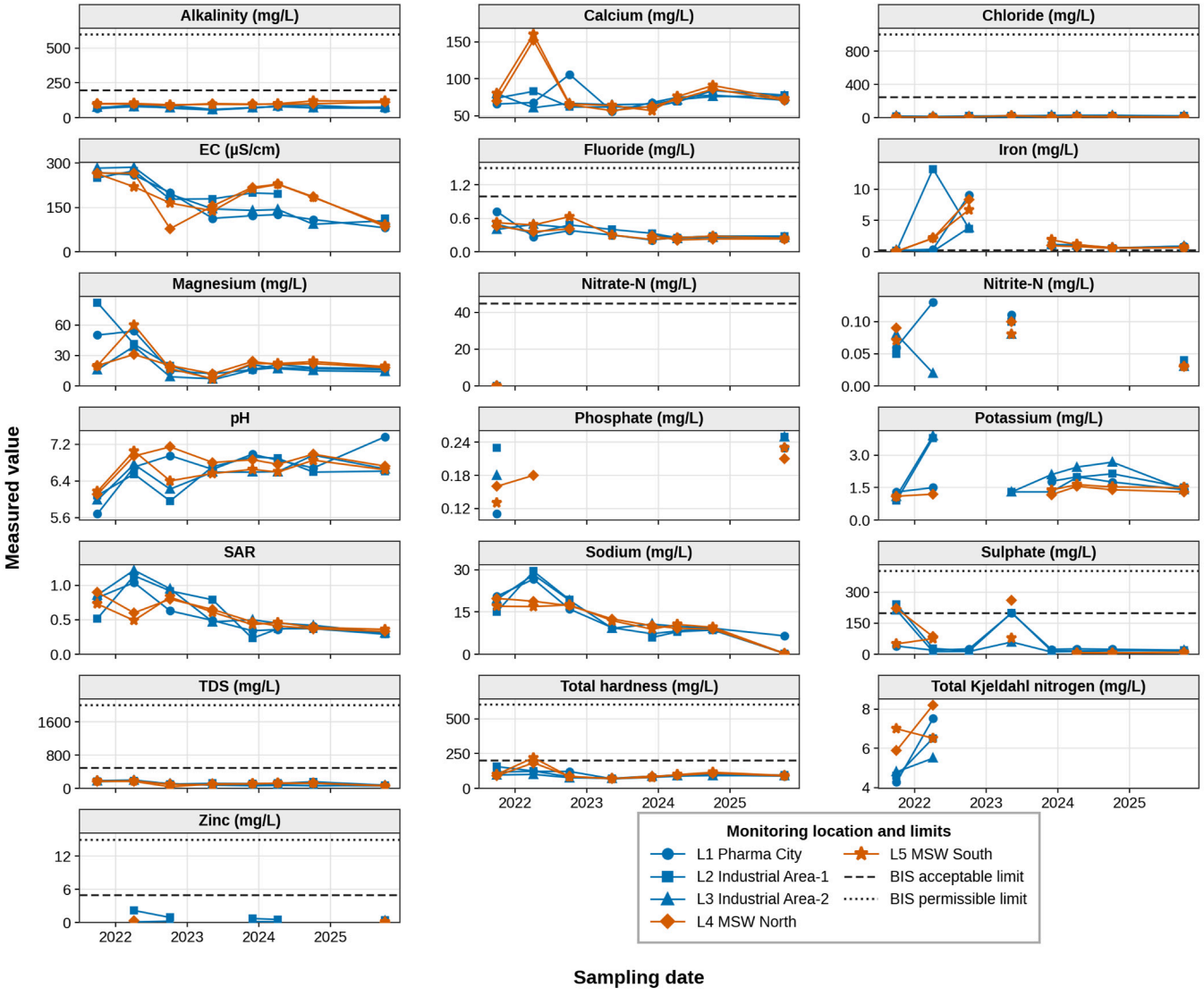


Figure 5. Temporal variation of key groundwater-quality parameters across the five monitoring locations in Dehradun (2021–2025). Dashed and dotted horizontal lines indicate the BIS IS:10500 (2012) acceptable and permissible limits, respectively, where such limits are defined. Values below the detection limit are not plotted, and the electrical conductivity value flagged in Table 1 (L2, October 2024) is omitted.

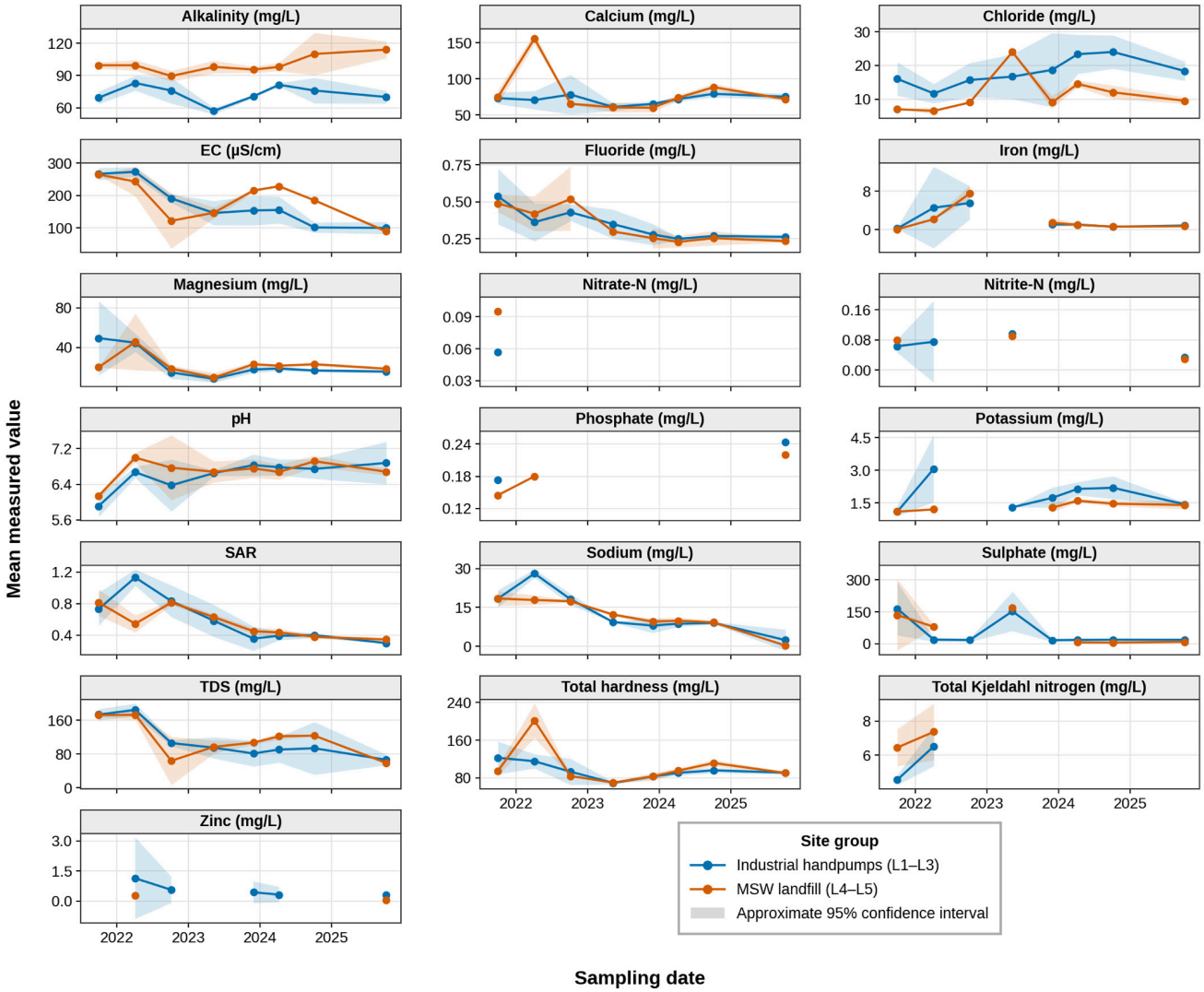


Figure 6. Mean temporal trends in groundwater-quality parameters across the industrial and municipal solid waste (MSW) site groups, showing pronounced fluctuations during the initial monitoring phase. Shaded bands show approximate 95% confidence intervals (mean ± 1.96 standard errors). Values below the detection limit are not included in the means, and the electrical conductivity value flagged in Table 1 (L2, October 2024) is omitted.

Applying a Benjamini–Hochberg false-discovery-rate correction correctly requires the full family of parameters tested for temporal trends, not only the subset that happened to reach nominal significance. Restricting the family to the parameters already flagged as significant in the narrative above would be circular and would understate the correction needed, so the full family of 23 parameters with non-zero variance was used instead, with *p*-values for every parameter in this family, including the eight listed above that were not part of the original narrative, computed directly from the underlying dataset using the same pooled OLS approach described above. Applying the Benjamini–Hochberg correction across this full family (m = 23, $\alpha = 0.05$) confirms that 13 of the 23 trends survive multiple-testing correction, ranked by *p*-value: sodium, sodium adsorption ratio, EC, total Kjeldahl nitrogen, TDS, fluoride, chromium, nitrate, pH, sulphate, magnesium, copper and nitrite. pH, TDS, EC, sulphate and sodium remain among the strongest and most robust of these; total hardness and chloride do not survive correction at this family size and should be interpreted with corresponding caution rather than treated as equivalent in strength to the other 13 trends. As a further sensitivity check, a season-adjusted OLS model (period index plus a pre-/post-monsoon season indicator) was fitted for the original seven narratively-

highlighted trends, and all seven retained materially unchanged significance status (within 0.02 of the pooled-model results reported above) under this adjustment; this check was not separately repeated for the eight additional trends identified through the full 23-parameter family-wise correction, which is noted as a direction for further robustness testing.

As a further robustness check, the same seven period-index trends were re-estimated using only the six continuous, evenly-spaced 2022–2024 monitoring rounds (periods 1–6 of 8), excluding the single 2021 and 2025 rounds for which seasonal and inter-annual effects cannot be separated (Section 4.4). TDS ($r = -0.41$, $p = 0.024$), EC ($r = -0.50$, $p = 0.005$), sodium ($r = -0.74$, $p < 0.001$) and chloride ($r = 0.46$, $p = 0.010$) remained significant on this restricted window. pH ($r = 0.16$, $p = 0.393$) and sulphate ($r = -0.22$, $p = 0.242$) did not, indicating that their full-period significance is driven substantially by the transition from the 2021 baseline to the 2022 rounds rather than by a continued trend across 2022–2024 alone. Total hardness was borderline on both windows ($p = 0.036$ full period, $p = 0.078$ restricted). The pH and sulphate findings should therefore be read as evidence of recovery from the 2021 episode specifically, rather than a continuing multi-year directional trend, while the TDS, EC, sodium and chloride trends appear more robustly continuous across the study period.

Box-and-whisker plots (Figure 7) and frequency distributions (Figure 8) show the distributional characteristics and outlier structure of each parameter by location. Sulphate and iron had the most pronounced positive skewness and outlier-driven distributions, and L2-Industrial Area-1 had the widest interquartile range for both, pointing to the highest temporal variability among all sites. The MSW landfill sites (L4, L5) had notably higher alkalinity values (median ~95–100 mg/L versus ~75 mg/L at the Selaqui sites), a pattern examined further in the Discussion.

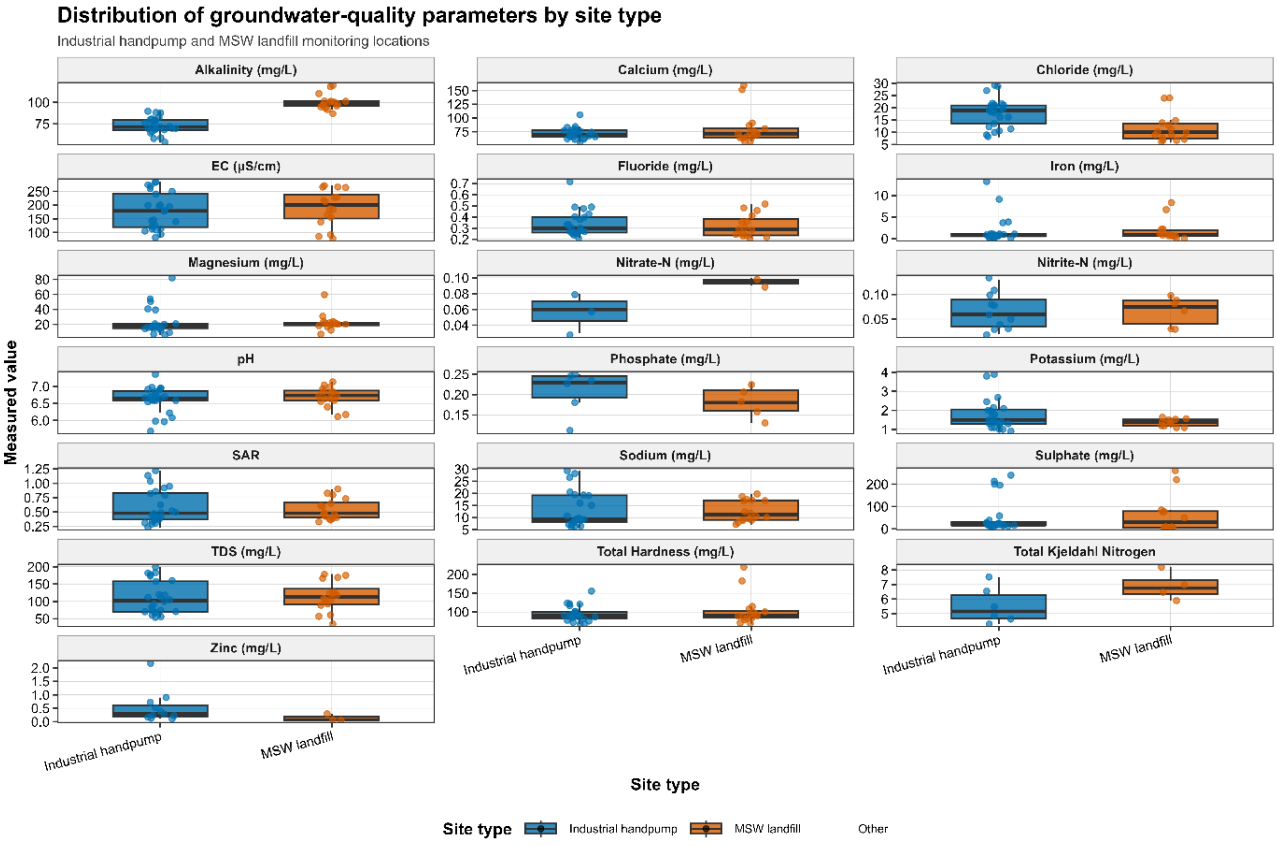


Figure 7. Box plots showing the relative variation in key parameters between the industrial and municipal solid waste (MSW) site groups (mean values). The industrial sites show greater variation in EC, chloride, nitrite, phosphate, SAR, sodium and TDS than the MSW sites.

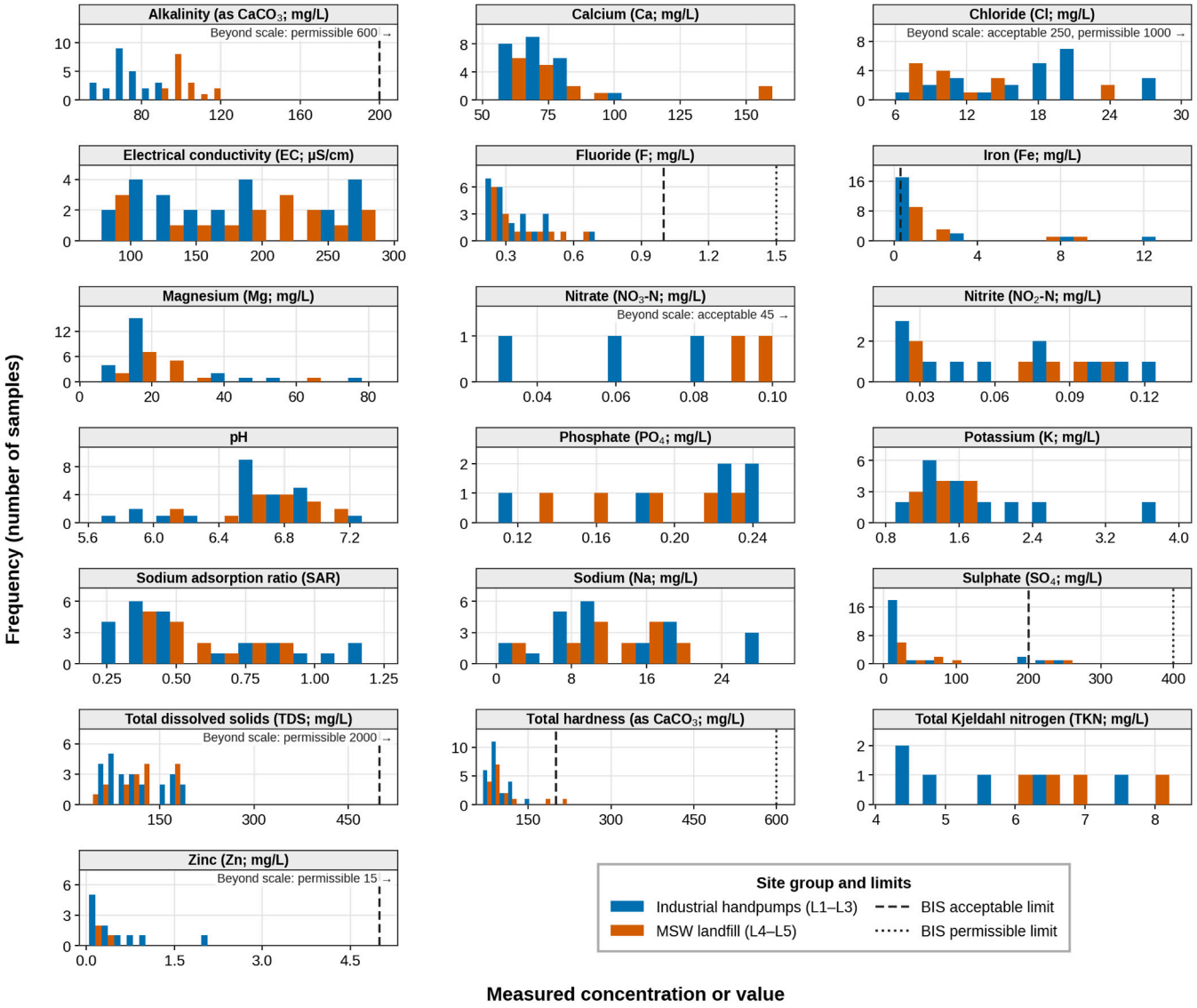


Figure 8. Frequency distribution charts of the major hydrochemical components for the industrial (L1–L3) and MSW landfill (L4–L5) sites. Dashed and dotted vertical lines mark the BIS IS:10500 (2012) acceptable and permissible limits, respectively. Where a limit lies beyond the plotted range, its value is given in the panel. Values below the detection limit are not included.

3.4. Inter-Parameter Correlations

The Pearson correlation matrix (Figure 9) revealed several meaningful hydrogeochemical relationships. TDS and EC were strongly correlated ($r = 0.95$, $p < 0.001$) after exclusion of a single implausible electrical-conductivity reading at site L2 in October 2024 that had substantially depressed the raw correlation coefficient. Total hardness was strongly correlated with both calcium ($r = 0.88$, $p < 0.001$) and magnesium ($r = 0.75$, $p < 0.001$), consistent with calcium and magnesium being the principal contributors to hardness. Total alkalinity, by contrast, showed only a weak positive correlation with total hardness ($r = 0.27$, $p = 0.10$), suggesting that carbonate dissolution and general mineralisation are only loosely coupled at these sites. Sulphate and sodium were weakly and non-significantly correlated ($r = 0.10$, $p = 0.54$). This indicates only that no statistically significant linear relationship was detected between the two ions, not that they necessarily derive from independent sources. Iron and pH showed a weak, non-significant positive correlation ($r = 0.09$, $p = 0.59$), which does not support pH-dependent iron precipitation as a controlling process across the dataset as a whole, though the mechanism may still operate locally at specific sites and sampling dates.

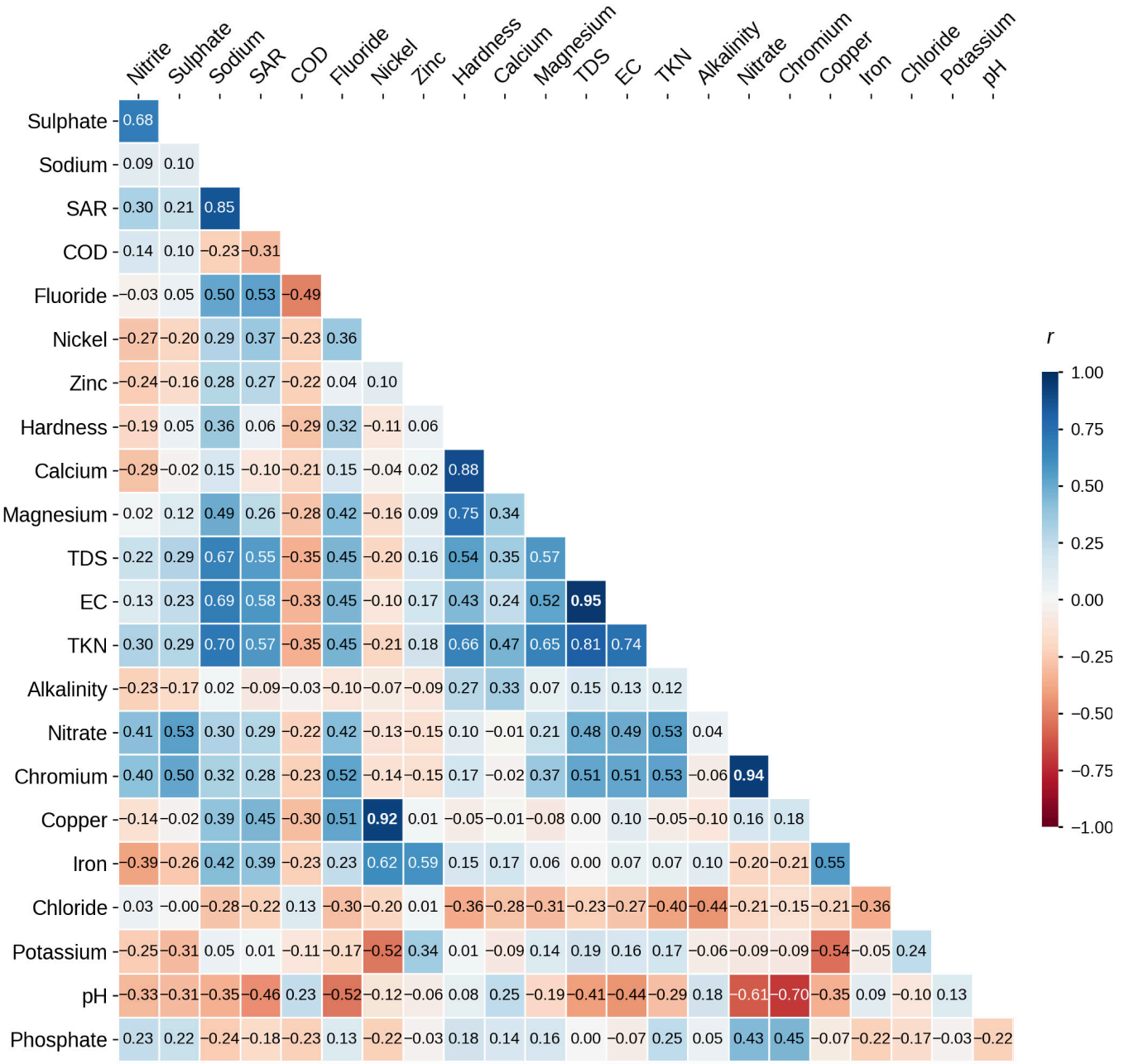


Figure 9. Pearson correlation matrix of the measured physicochemical and trace-metal parameters.

Correlations among nickel, zinc and copper were recomputed for the full dataset using the zero-substitution convention applied to all non-detects, rather than being restricted to the small subset of paired non-zero detections used in the original analysis. That earlier restriction left as few as two paired observations for some metal pairs—a sample size at which the Pearson correlation coefficient is mathematically constrained to plus or minus one regardless of the true underlying relationship—and produces apparent values of r = 1.00 and r = −1.00. Using the full sample, nickel and copper are strongly correlated (r = 0.92), consistent with both metals being detected together at all five sites in the post-monsoon 2022 round and at no other time; nickel–zinc (r = 0.10) and zinc–copper (r = 0.01) show no comparable relationship, because zinc's detections are distributed across different rounds and sites than the nickel–copper co-occurrence. Because the nickel–copper correlation rests on a single shared detection event rather than a continuous concentration gradient, it is

best read as evidence of a shared trace-metal episode in that round rather than a general geochemical association.

3.5. Inter-Location Statistical Comparisons

The principal component analysis was restricted to the 14 parameters with a detection frequency of at least 65% (pH, TDS, EC, hardness, calcium, magnesium, alkalinity, chloride, fluoride, sulphate, sodium, potassium, SAR and iron; Figure 10). Nitrate, nitrite, phosphate, COD, TKN, copper, zinc, nickel and chromium were excluded from the PCA because their high non-detect frequencies would make their treatment as continuous standardised PCA inputs unstable. On this reduced, reliably-measured parameter set, the first principal component (PC1, 34.0% of variance) was dominated by positive loadings of TDS, EC, sodium and magnesium, pointing to general salinity and mineralisation, while the second principal component (PC2, 17.4% of variance) was dominated by positive loadings of calcium, hardness and alkalinity against negative loadings of chloride, sulphate and SAR, a carbonate-hardness axis. Because several input variables are mathematically related (TDS and EC, hardness with calcium and magnesium, and SAR with sodium, calcium and magnesium), these redundancies shape the loadings, and the ordination is interpreted as exploratory only. MSW-associated sites tended to score higher on PC2 than industrial sites in this ordination, matching the stronger bicarbonate signature already identified at these sites by the Piper diagram (Figure 11). Because only three industrial and two landfill wells were repeatedly sampled, treating the 40 measurements as independent replicates for a formal between-group test would overstate the effective sample size, in the same way already flagged for the pooled trend model above. This pattern is therefore reported descriptively rather than significance-tested, and formal inference about site-group differences instead relies on the properly repeated-measures Friedman test and the Piper diagram (Figure 11). The first two principal components jointly explained 51.3% of total variance, but the two site groups still overlap substantially in ordination space and no confirmatory factor structure is implied by a sample of this size. This result is therefore best read as an exploratory ordination that supports the carbonate-hardness contrast already established by the Piper diagram, rather than as independent evidence of source apportionment.

Kruskal–Wallis H-tests comparing the five sites were run for the twelve reliably-measured physicochemical and major-ion parameters (pH, TDS, EC, hardness, calcium, magnesium, alkalinity, chloride, fluoride, sulphate, sodium and SAR). Total alkalinity differed significantly among sites ($H = 27.4$, $df = 4$, $p < 0.001$), and so did chloride ($H = 13.0$, $df = 4$, $p = 0.011$); no other parameter reached significance (all $p > 0.14$). Because the same five sites were sampled repeatedly across the eight monitoring rounds, the Kruskal–Wallis test's assumption of independent observations is not strictly met. A Friedman test treating monitoring round as a blocking factor was therefore run as a robustness check. It confirmed the alkalinity ($\chi^2 = 22.9$, $p < 0.001$) and chloride ($\chi^2 = 14.3$, $p = 0.006$) differences, and further identified a significant site effect for magnesium ($\chi^2 = 12.1$, $p = 0.017$) and a borderline effect for sulphate ($\chi^2 = 10.0$, $p = 0.040$) once the repeated-measures structure was accounted for, neither of which reached significance under the simpler Kruskal–Wallis test. The alkalinity and chloride differences match the stronger bicarbonate signature and lower chloride contribution already reported at the MSW-associated sites in the Piper diagram (Figure 11) and PCA above. Unlike the temporal trend p-values in Section 3.3, these Kruskal–Wallis and Friedman test results across twelve parameters have not been corrected for multiple comparisons, so some of the nominally significant findings reported here, particularly the borderline sulphate effect, may not survive such a correction and are reported as exploratory rather than confirmatory.

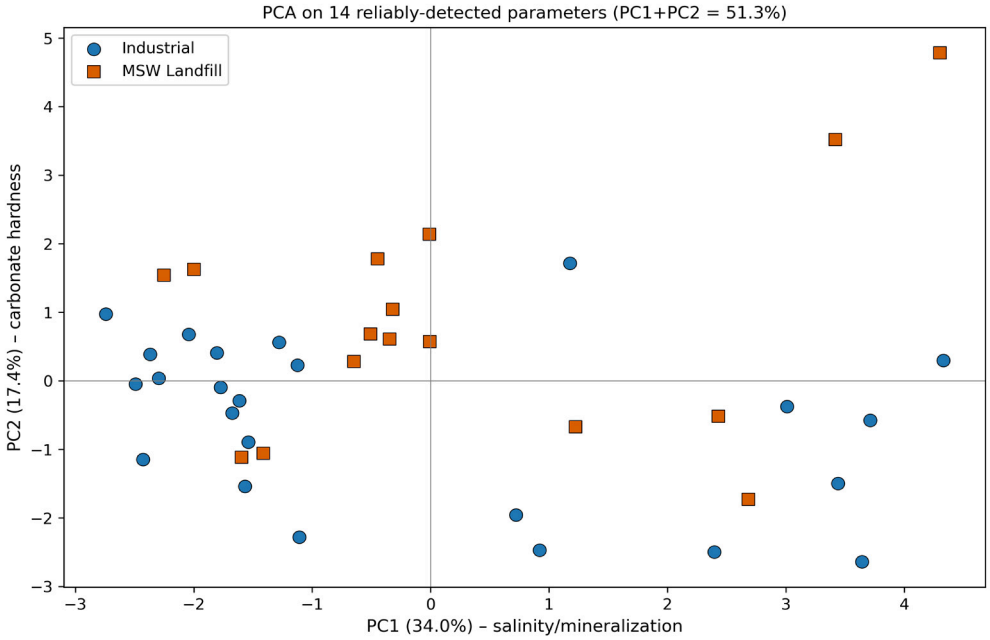


Figure 10. Principal component analysis (PCA) score plot of the 40 site-period observations, computed from the 14 reliably detected water-quality parameters (detection frequency ≥65%). Each point is one site-period observation, coloured by site group. MSW-associated sites tend to score higher on PC2 than industrial sites, consistent with the carbonate-hardness contrast identified by the Piper diagram (Figure 11).

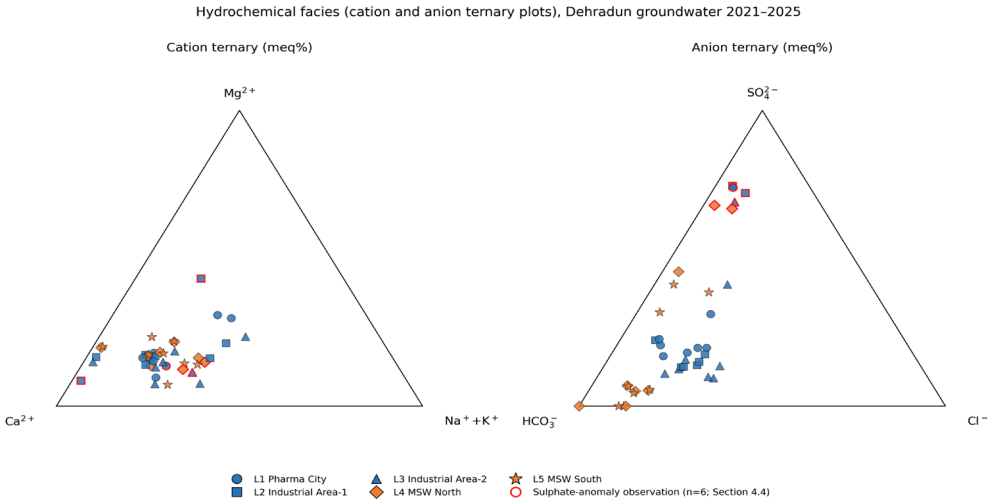


Figure 11. Piper trilinear diagram of major-ion hydrochemistry (cation and anion ternary plots), Dehradun groundwater, 2021–2025. Most individual samples (27/34 after excluding the six sulphate-anomaly observations discussed in Section 4.4) plot within the Ca-HCO_3 facies field; the remainder are mixed-cation and/or mixed-anion compositions rather than a single uniform facies (Section 3.5). Red-outlined symbols mark the six sulphate-anomaly observations.

Sample-level hydrochemical facies classification (dominant ion defined as exceeding 50% of total cation or anion equivalents) found that 27 of the 40 individual observations (67.5%) plot in the Ca-HCO_3 facies, with four mixed-cation/HCO_3, two Ca-dominant/mixed-anion, one fully mixed, and six SO_4-dominant or mixed-SO_4 compositions (Figure 11); the six SO_4-leaning observations correspond exactly to the six sulphate/TDS data-quality flags discussed in Section 4.4, so this facies pattern should be read alongside that caveat rather than as independent evidence of a distinct hydrochemical process. This facies classification is based on each ion's relative share of total cation

or anion equivalents rather than on whether the ion was reliably detected across samples. Sodium, potassium and chloride, for example, were detected in the large majority of samples (Section 2.3) even though none of them dominates the equivalent-percentage totals that define the facies groups reported above. Sample-level ionic charge-balance error (CBE% = 100 × (Σcations − Σanions)/(Σcations + Σanions), computed in meq/L using the corrected elemental calcium and magnesium values) ranged from −61.7% to +21.8% (mean −8.6%) across the 40 observations; 22 of 40 (55%) fall within the conventional ±10% acceptance band and 26 of 40 (65%) within ±15%. The four largest charge imbalances (−43.0% to −61.7%, all anion-excess) belong to the Oct-2021 L4 and May-2023 L1/L2/L4 observations, coinciding with four of the six sulphate/TDS flags and providing independent, charge-balance-based corroboration that those specific observations are analytically suspect; the remaining 36 observations have a mean CBE of −3.5%.

3.6. Water Quality Index and Heavy Metal Pollution Index

A Water Quality Index (WQI) was calculated for each site and monitoring period using a weighted arithmetic approach adapted from Brown et al. [24], based on nine parameters with established BIS IS:10500 (2012) acceptable limits (pH, TDS, total hardness, calcium, magnesium, chloride, sulphate, nitrate and fluoride). Unit weights were assigned as wi = K/Si, where Si is the BIS acceptable limit for parameter i and K is a proportionality constant equal to the reciprocal of the sum of 1/Si across all included parameters. The resulting WQI classified all site-period combinations as excellent (WQI < 50) or good (50 ≤ WQI < 100). Major-ion chemistry was therefore generally favourable across sites and periods (Table 2).

Table 2. Water Quality Index (WQI) and Heavy Metal Pollution Index (HPI) summary by site, 2021–2025 (*n* = 8 monitoring periods per site). HPI critical threshold = 100 [26]. Full site- and period-level values are provided in Tables S1 and S3.

Site	WQI Range	HPI Range	Periods with HPI ≥ 100
L1 Pharma City	19–88	0–891	2 of 8
L2 Industrial Area-1	24–62	0–925	3 of 8
L3 Industrial Area-2	9–55	0–664	2 of 8
L4 MSW North	5–57	0–816	2 of 8
L5 MSW South	26–65	0–667	2 of 8

Because trace metals are not represented in the major-ion WQI, a complementary Heavy Metal Pollution Index (HPI) was calculated following Mohan et al. [26] for iron, copper, nickel, chromium and zinc, the five trace metals with measurable concentrations in this dataset (Table 2). As with the WQI, lower HPI values indicate better water quality. Following Mohan et al. [26], HPI below 30 is classed as low, 30–99 as high and 100 or above as critical, so a value below 100 is sub-critical but not necessarily acceptable. The critical threshold of 100 marks a composite index-based measure of heavy metal pollution rather than a direct toxicological or health-risk assessment; health risk from the same metals is evaluated separately, using the standard USEPA framework, in Section 3.7. The HPI exceeded the critical value of 100 in 11 of the 40 site-period observations: all five sites in the 2021 baseline, all five sites in the post-monsoon 2022 round, and L2-Industrial Area-1 alone in the intervening pre-monsoon 2022 round. The most severe episode, by HPI magnitude, occurred in the post-monsoon 2022 period, when all five sites recorded HPI values between 664 and 925. Full metal-specific hazard quotients and concentrations for every site and period are given in Tables S2 and S3, allowing each metal to be checked individually against its own regulatory limit rather than relying on the summed index alone. Decomposing the HPI into its metal-specific components shows this episode was

driven almost entirely by nickel (84–92% of the HPI at every site), which, like chromium in 2021, was detected only in this single round. The 2021 baseline critical episode, by contrast, was driven almost entirely by chromium (88–96% of the HPI at every site). Iron was the dominant HPI component in only one of the eleven critical site-period observations (L2-Industrial Area-1, pre-monsoon 2022, 99.9% of the HPI). The high peak HPI values reported in Table 2 (up to the high hundreds) reflect this same weighting effect: because each metal's sub-index is scaled inversely to its own, often very strict, regulatory limit, a concentration several-fold above the limit for nickel or chromium produces a correspondingly large index contribution rather than indicating an error in the underlying concentration data. Despite its high absolute concentrations at several sites and periods, iron's comparatively lenient regulatory standard (0.3 mg/L, against 0.02 mg/L for nickel and 0.05 mg/L for chromium) means it contributes only a small fraction of the weighted HPI even when substantially elevated. HPI values fell below 30 at every site from 2023 onward, mirroring the declining sulphate trend and the declining, though not statistically significant, iron trend. Heavy metal pollution therefore represented the principal water quality concern at all five sites during the early monitoring period, driven by different trace metals at different points in the monitoring period rather than by a single persistent contaminant—a pattern that the major-ion WQI alone does not capture.

The "below 30" classification reported above for 2023–2025 depends on the zero-substitution convention adopted for non-detects. Repeating the HPI calculation with the laboratory-documented detection-limit sensitivity check described in Section 2.3 (half of each metal's own documented detection limit substituted for every zero reading in copper, nickel, chromium and zinc) leaves all 11 already-critical site-periods critical, and moves every one of the remaining 29 site-periods—all those previously classified "low"—directly into the "critical" band (HPI 152.9–178.8), including every site from 2023 onward; under this convention, all 40 site-period observations in the dataset classify as critical. This shows that the reassuring "low" classification for the post-2022 period is highly sensitive to the assumed non-detect convention: using the source laboratory's own documented detection limits, the apparent improvement in heavy metal water quality from 2023 onward does not hold, and the zero-substitution result should accordingly be read as an assumption-dependent lower bound rather than a confirmed water-quality status.

3.7. Human Health Risk Assessment

The hazard index (HI) for combined ingestion of copper, zinc, nickel and chromium exceeded the safety threshold of 1 at all five sites in the 2021 baseline period, for both adults (HI 7.93–10.06) and children (HI 18.49–23.46), driven almost entirely by chromium, which was detected only in this period (0.26–0.33 mg/L at all sites) and in no other of the eight monitoring rounds. Copper, zinc and nickel are retained in the combined index alongside chromium because USEPA's hazard index approach is defined as the sum of hazard quotients across all co-occurring metals of concern rather than a single-metal assessment, even in periods such as 2021 where one metal dominates the total. These hazard-index values use the current (August 2024) [33] USEPA IRIS chromium(VI) oral reference dose of 9×10^{-4} mg/kg-day. The previously standard value of 0.003 mg/kg-day would understate the 2021 hazard index by a factor of roughly 3.3. As the sensitivity check promised in Section 2.3, substituting the trivalent chromium reference dose (1.5 mg/kg-day) for the hexavalent value reduces the 2021 hazard index to 0.016–0.031 in adults and 0.036–0.071 in children, i.e., from roughly an order of magnitude above the safety threshold of 1 to two orders of magnitude below it. Because the actual Cr(VI)/Cr(III) speciation was not measured, the hazard-index values above should be read as a conservative upper bound under a worst-case speciation assumption rather than a confirmed risk level; the true risk lies somewhere between

these two bounds depending on the unmeasured actual speciation. A screening-level incremental lifetime cancer risk (ILCR = LADD × CSF), computed using the 2024 IRIS oral cancer slope factor for hexavalent chromium (0.16 (mg/kg-day)$^{-1}$) and the same worst-case total-chromium-as-Cr(VI) assumption, ranged from 4.9×10^{-4} to 6.2×10^{-4} across the five sites under an upper-bound screening assumption of a full 30-year adult exposure at the 2021 concentration, several times above USEPA's upper acceptable-risk bound of 10^{-4}. Because chromium was detected only in a single monitoring round, this 30-year duration is a bounding screening assumption rather than an exposure duration established by the monitoring record; under an alternative, shorter bounding scenario of one year of exposure at the same concentration, the resulting ILCR (1.6×10^{-5} to 2.1×10^{-5}) falls within USEPA's 10^{-6}–10^{-4} risk-management range. Neither duration is supported by the monitoring record itself, which cannot distinguish a one-year exposure from a longer or shorter one; both are presented only as bounding scenarios rather than observed exposure durations. No corresponding cancer-risk sensitivity analysis is possible under the trivalent assumption, because USEPA has not established an oral cancer slope factor for Cr(III), which is not classified as carcinogenic by the oral route. This screening result should not be read as a confirmed lifetime risk, since both its duration and its speciation assumptions are upper-bound screening choices rather than observations, but it indicates that the 2021 chromium episode calls for confirmatory speciation sampling rather than dismissal as a data artefact. A smaller, child-only exceedance occurred in the post-monsoon 2022 period at two sites (L1 Pharma City, HI = 1.02; L2 Industrial Area-1, HI = 1.31), driven by nickel, which was likewise detected only in this single period (0.21–0.32 mg/L at all five sites). From 2023 onward, HI remained at or below 0.15 for both receptors at every site, and adults did not exceed HI = 1 in any period other than 2021 (Table 3).

Table 3. Human health risk assessment summary by site: peak hazard index (HI) for combined ingestion of copper, zinc, nickel and chromium, and number of monitoring periods (of eight) exceeding the safety threshold HI = 1, by receptor. Full site-, period- and receptor-level values are provided in Table S2.

Site	Adult HI (Max)	Adult Periods HI > 1	Child HI (Max)	Child Periods HI > 1
L1 Pharma City	8.5	1 of 8	19.9	2 of 8
L2 Industrial Area-1	9.4	1 of 8	22.1	2 of 8
L3 Industrial Area-2	9.8	1 of 8	22.8	1 of 8
L4 MSW North	7.9	1 of 8	18.5	1 of 8
L5 MSW South	10.1	1 of 8	23.5	1 of 8

As with the Heavy Metal Pollution Index above, this "at or below 0.15" range depends on the zero-substitution convention for non-detects. Repeating the hazard-index calculation with the laboratory-documented detection-limit sensitivity check (Section 2.3) raises HI to 0.992–1.190 in adults and 2.316–2.777 in children across the pre-monsoon 2022 and 2023–2025 periods (the six rounds not already separately reported as critical in Sections 3.6 and 3.7); under this convention, HI_child exceeds 1 in all 30 of these site-period observations, and HI_adult also exceeds 1 in 10 of the 30 (chiefly at L2 and L3 Industrial Area, with isolated exceedances at L1 and L4), driven primarily by the assumed chromium and nickel concentrations at this sensitivity level. These results now rest on the source laboratory's own documented detection limits (Supplementary Table S5) which gives them substantial weight; they indicate that chronic low-level exposure risk from these four metals, particularly for children, may be understated by the zero-substitution convention across most of the post-2021 monitoring period, and are reported here, together with the

actual detection limits now available (Section 4.4), as a reason to treat the "at or below 0.15" zero-substitution result as a lower bound rather than a confirmed finding.

3.8. Irrigation Water Quality Suitability

Kelly's ratio (the ratio of sodium to the sum of calcium and magnesium, defined in Section 2.3, computed from the corrected elemental calcium and magnesium concentrations) ranged from 0.00 to 0.61 (mean 0.27) across all samples, well below the suitability threshold of 1. Percent sodium ranged from 2% to 40% (mean 21%), below the 60% unsuitability threshold throughout. Residual sodium carbonate, a derived balance of bicarbonate against calcium plus magnesium rather than a measured concentration, ranged from −2.36 to 0.64 meq/L (mean −0.29), safely below the 1.25 meq/L hazard threshold at every site and period; a negative RSC value, which predominates across the dataset, is the favourable outcome for this index and indicates no carbonate hazard. Magnesium hazard ranged from 9% to 53% (mean 22%), exceeding the 50% caution threshold in a single observation (L2 Industrial Area-1, October 2021), rather than the several samples that an uncorrected calculation using total hardness would suggest. The permeability index of Doneen (Section 2.3) classified 22 of 40 samples (55%) as Class I (excellent) and the remaining 18 (45%) as Class II (good), with no sample falling into the unsuitable Class III and no consistent temporal or spatial pattern (Table 4). A USSL salinity-alkali classification (Figure 12) placed all samples within the low-salinity (C1–C2) and low-sodium-hazard (S1) categories, the most favourable classes in the USSL scheme. Groundwater at all five sites therefore falls within the most favourable USSL salinity-alkali classes throughout the monitoring period; because low-EC water can still present an infiltration-rate problem depending on SAR and soil structure, EC and SAR should nonetheless be evaluated jointly (Section 4.2) rather than treating these favourable individual indices alone as confirmation of unrestricted suitability.

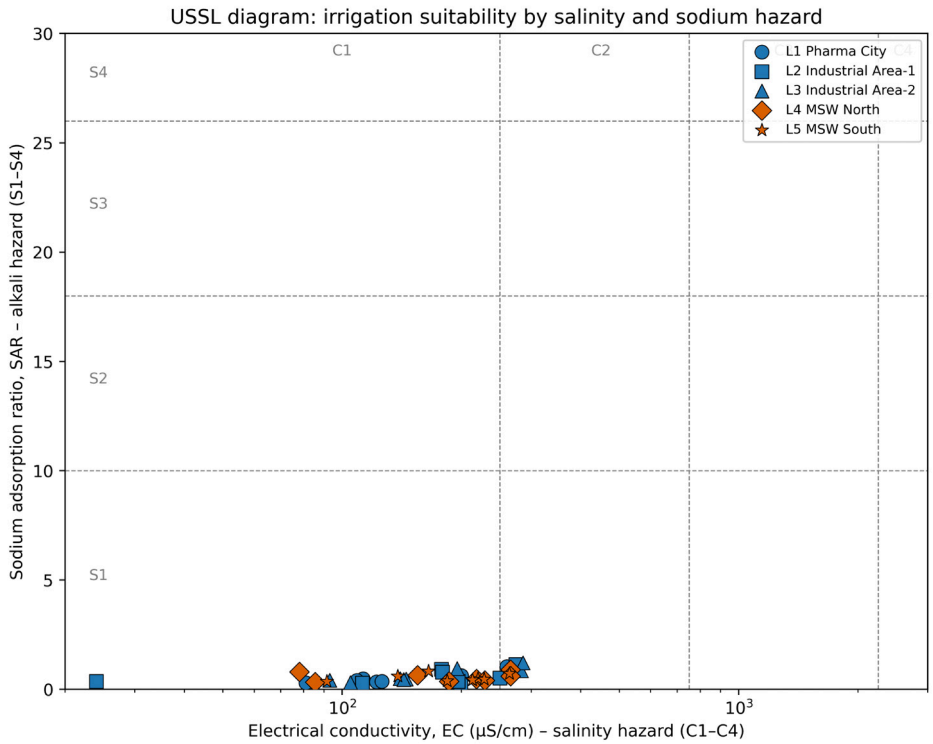


Figure 12. USSL diagram plotting sodium adsorption ratio (SAR, *y*-axis) against electrical conductivity (EC, *x*-axis) and classifying irrigation suitability by salinity hazard (C1–C4) and sodium/alkali hazard (S1–S4). All samples plot within the C1–C2/S1 region.

Table 4. Irrigation water quality suitability indices by site (range across the eight monitoring periods, 2021–2025). PI class: I = excellent, II = good [30]. USSL salinity-alkali classification (Figure 12) placed all samples in class C1–C2/S1 for every site.

Site	Kelly's Ratio	Mg Hazard (%)	Na (%)	RSC (meq/L)	Doneen PI Class
L1 Pharma City	0.16–0.47	12.4–44.3	15.3–32.9	−1.04 to −0.18	2 × I, 6 × II
L2 Industrial Area-1	0.00–0.52	8.8–52.6	2.4–35.7	−1.72 to −0.08	4 × I, 4 × II
L3 Industrial Area-2	0.01–0.61	9.7–39.0	2.5–39.9	−0.44 to −0.08	4 × I, 4 × II
L4 MSW North	0.01–0.48	16.9–27.6	2.3–33.1	−1.72 to 0.64	6 × I, 2 × II
L5 MSW South	0.01–0.46	9.9–27.9	2.6–31.5	−2.36 to 0.52	6 × I, 2 × II

4. Discussion

4.1. Hydrogeochemical Interpretation, Heavy Metal Pollution and Health Risk

The groundwater geochemistry in the study area is predominantly consistent with a Ca-HCO_3 hydrogeochemical facies (Section 3.5), typically associated with calcite dissolution, with a minority of samples showing mixed-cation or mixed-anion compositions. Strong calcium hardness and a weak alkalinity-hardness association are consistent with this geogenic baseline, although saturation-index or ionic-ratio evidence would be needed to confirm mineral dissolution directly rather than inferring it from the Piper classification alone. The mechanisms discussed below (pyrite oxidation, reductive iron dissolution and leachate-derived inputs) are proposed as plausible hypotheses consistent with the observed patterns. In the absence of background wells, groundwater-flow data, isotopic tracers or direct leachate/effluent analyses, they cannot be established as confirmed sources or processes. The elevated sulphate and depressed pH observed at L1 and L2 in 2021 are consistent with early-stage pyrite oxidation ($FeS_2 + 7/2O_2 + H_2O \rightarrow Fe^{2+} + 2SO_4{}^{2-} + 2H^+$), possibly alongside changes in wastewater inputs during this period and local hydrogeochemical conditions. Measured dissolved iron at L1 in 2021 was low (0.18 mg/L), which at first looks inconsistent with this mechanism. However, Fe^{2+} generated by pyrite oxidation oxidises and precipitates as $Fe(OH)_3$ rapidly once it reaches near-neutral, oxic conditions near the well head, so a transient Fe^{2+} pulse would not necessarily be captured by a point-in-time dissolved iron measurement. The much larger iron concentrations recorded at L1 and L2 in 2022 occurred at near-neutral pH (6.55–6.95) and may instead reflect a separate process, most plausibly localised reductive dissolution of iron oxides under episodically reducing conditions, or physical disturbance of the well during purging that mobilised particulate iron ahead of sampling. Distinguishing between these mechanisms would require paired redox-potential and filtered/unfiltered iron measurements, which were not available in the secondary dataset used here and are recommended for future monitoring rounds. The higher iron values at the MSW sites L4 and L5 are instead consistent with reductive dissolution by organic matter from leachate, proposed here as a hypothesis ($4Fe(OH)_3 + CH_2O + 7H^+ \rightarrow 4Fe^{2+} + HCO_3{}^- + 10H_2O$; mass- and charge-balanced).

Piper trilinear analysis of the major-ion composition (Figure 11), using the corrected elemental calcium and magnesium concentrations (Section 2.3), classified each of the 40 individual site-period samples separately rather than relying on site-average composition. Calcium contributed 37–89% (mean 62%) and magnesium 7–43% (mean 17%) of total cation equivalents across the dataset. Seven samples—all from the October 2021 and May 2023 rounds at L1–L4—plot in the sulphate-dominated portion of the anion triangle (sulphate 41–75% of anion equivalents) rather than the bicarbonate-dominated field seen elsewhere; six of these coincide exactly with the sulphate measurements that exceed the corresponding TDS value for the same sample (Section 4.4), so they are treated together with that data-quality concern rather than as evidence of a genuine sulphate-dominated facies. Restricting the classification to the 34 samples without a flagged sulphate value,

27 (79%) are Ca-HCO_3 facies, four are mixed-cation/HCO_3, two are Ca-dominant with a mixed-anion signature, and one is fully mixed; a single facies therefore cannot be assumed to hold at every site and every sampling round, and facies should be read at the level of the individual observation. Among these 34 samples, bicarbonate contributed a higher share of anion equivalents at the MSW-associated sites (L4, L5: mean 76%, range 45–100%) than at the industrial cluster (L1–L3: mean 61%, range 39–71%), with correspondingly lower chloride (mean 10% vs. 21%). This pattern is not fully consistent with a typical leachate signature, which would usually elevate chloride alongside alkalinity, so it may instead reflect differing background carbonate geochemistry between the two site groups rather than a confirmed leachate contribution. Direct leachate indicators such as ammonium and dissolved organic carbon were not measured in this dataset, so a leachate origin for the elevated alkalinity at L4 and L5 cannot be confirmed here and is noted as an open question in Section 4.4. Despite this generally favourable major-ion picture, the Heavy Metal Pollution Index results show that all five sites experienced at least one period of critical values, driven by chromium in 2021 and by nickel in the post-monsoon 2022 round rather than by iron. This is a clear argument for reporting the two indices separately rather than combining trace metals and major ions into a single composite score.

The human health risk assessment offers a complementary, risk-based reading of the same trace-metal concentration data. Elevated hazard indices occurred within the same 2021–2022 trace-metal episode identified by the HPI, though the site-specific patterns were not identical. The hazard index exceeded the safety threshold at all five sites in 2021 and, for children, at two sites in post-monsoon 2022, even though major-ion water quality and irrigation suitability were generally favourable throughout the rest of the study.

4.2. Environmental Interpretation

Higher iron concentrations are an aesthetic problem (metallic taste, staining) and can inhibit biological processes in soil ecosystems, reducing microbial diversity and enzymatic activity important for nitrogen cycling, in keeping with meta-analytic evidence that trace-metal loading disproportionately suppresses microbially mediated soil enzyme activity relative to other soil functions [34]. Sustained irrigation with iron-rich groundwater can, in principle, promote ferruginous crusting at the soil surface, which would reduce hydraulic conductivity and impede plant root aeration, although this has not been directly measured at the study sites and the concentrations observed here have not been shown to reach a threshold at which such crusting occurs. Iron-plaque formation on root surfaces—a related but distinct process—has been shown experimentally to reduce shoot growth and disrupt phosphorus translocation to leaves in wetland plant species grown in pot experiments using natural lake sediments of varying iron and iron-phosphorus content, even where the plaque itself causes no visible root damage, with the severity depending on the sediment's iron and iron-phosphorus content rather than on iron concentration alone [35]. Sulphate was generally below the BIS guideline but episodically exceeded 200 mg/L at several sites, which is agronomically relevant even though it does not operate through soil acidification. Microbial sulphate reduction ($SO_4^{2-} \rightarrow H_2S$) consumes protons and generates alkalinity rather than acidity, and is in fact the mechanism exploited to raise pH in passive bioremediation of acidic, metal-contaminated waters, so it is not invoked here as a soil-acidification pathway. The acidification observed at L1 and L2 in 2021 could instead fit pyrite oxidation or other localised acid-generating processes, chemically opposite to sulphate reduction, though this cannot be confirmed without direct mineralogical or isotopic data. Sulphate therefore plays a double-edged agronomic role. It is itself an essential plant macronutrient, taken up by roots almost exclusively as sulphate and required for amino acid (cysteine, methionine), protein and chlorophyll synthesis, so sustained

sulphate deficiency and episodic sulphate enrichment from acid-generating processes sit at opposite ends of the same nutrient-management concern at these irrigation-dependent sites. More than 95% of soil sulphur is held in organic, microbially mineralised forms rather than as directly plant-available sulphate at any given time [36]. The chromium and nickel episodes identified during the early monitoring period are relevant to soil biological function as well as human health. Laboratory and meta-analytic evidence show that trace metals including chromium, nickel, copper and zinc inhibit key soil enzymes, most strongly dehydrogenase and arylsulfatase activity (reductions on the order of 60–70% under elevated metal loading), and suppress microbial biomass and functional diversity even at concentrations below phytotoxic thresholds, with the degree of inhibition moderated by soil clay content and depth [34,37]. Because no soil measurements were available, the duration and reversibility of any associated soil biological effects cannot be inferred from the groundwater time series used here. The minimal nitrate observed, despite the adjacent agricultural and urban land use, is consistent with either effective natural denitrification or low anthropogenic nitrogen inputs, presented here as alternative hypotheses rather than a confirmed mechanism at the aquifer depth sampled, and the initial drop and later rise in pH is best attributed to the natural chemistry of the aquifer discussed above.

Groundwater is an important irrigation source in this peri-urban setting, and the very low SAR and chloride concentrations point to negligible sodium-hazard or salinity risk to soils across the monitoring period. The main irrigation-related concern is the episodic elevated iron loading seen during the early monitoring period, rather than a consistently high iron level. The soil-crusting and root-zone mechanisms by which sustained iron-rich irrigation could affect crop productivity are discussed in Section 4.2; monitoring the forms of iron present and the redox conditions would help track this risk in practice. Because iron oxidation-reduction cycling in soils is itself largely microbially mediated, the episodic iron loading identified here is mechanistically linked to the soil microbial and enzymatic effects discussed above, and sustained iron inputs at these levels would likely compound, rather than act independently of, the trace-metal-related suppression of soil enzyme activity reported in the wider contamination literature [34]. This qualitative picture is confirmed by the quantitative irrigation-suitability indices reported in Section 3.8, all of which classify the groundwater as favourable on sodium- and salinity-hazard grounds throughout the monitoring period; as detailed below, however, the Food and Agriculture Organization (FAO) EC-SAR joint evaluation gives a more cautious reading of infiltration suitability specifically. Electrical conductivity was consistently low across the dataset (78–286 µS/cm after excluding one flagged value of 24 µS/cm) and SAR low (0.23–1.22), placing groundwater at all five sites within the most favourable USSL salinity-alkali classes (C1–C2, low sodium hazard) throughout the monitoring period. FAO irrigation-water guidance [38] notes that low-EC water can nonetheless present an infiltration-rate problem depending on SAR and soil structure, so EC and SAR should be evaluated jointly rather than treating a low EC alone as confirmation of suitability. Although all samples plot within the C1–C2/S1 classes in the USSL diagram, the FAO EC-SAR framework gives a more cautious interpretation of infiltration suitability: because SAR remained below 3 throughout the dataset (0.23–1.22), samples with EC between 0.20 and 0.286 dS/m fall within the slight-to-moderate infiltration-restriction category, and samples with EC below 0.20 dS/m fall within the severe-restriction category. The low salinity and sodium hazard therefore do not by themselves imply unrestricted irrigation suitability, and site-specific soil conditions should be considered before unrestricted use.

4.3. Comparison with Previous Studies

The predominantly Ca-HCO_3 hydrochemical facies identified here through Piper trilinear analysis broadly matches Dudeja et al. [20], who established a Ca-Mg-HCO_3 facies from a single spatio-seasonal survey of 76 sources across the wider Doon Valley, although the present dataset shows calcium rather than magnesium as the dominant cation on average, a difference that may reflect the narrower, pressure-zone-specific sampling frame used here relative to their valley-wide survey. The present results extend this finding across eight monitoring rounds spanning five years rather than a single snapshot in time, while also showing, at the level of individual samples, that this facies is not uniformly stable. Besides the six sulphate-anomaly observations excluded above (Section 4.4), a further minority of observations (7/40), concentrated in the earlier monitoring rounds (periods 0–3, 2021–2023) rather than attributable to the sulphate data-quality issue, show mixed-cation or mixed-anion compositions rather than a classic Ca-HCO_3 signature. The major-ion Water Quality Index results, classifying groundwater as excellent to good at all sites and periods, closely match Pundir et al. [18], who reported 96% of sources across the valley as excellent to good using a comparable weighted arithmetic approach, and are broadly consistent with the district-level classification of Uttarakhand groundwater as predominantly excellent to good reported by Pandey et al. [22] across the wider Western Himalayan region.

The Heavy Metal Pollution Index results present a more contrasting picture. Nayak et al. [21], sampling the Selaqui industrial belt during a single monitoring round, reported HPI values in the high but sub-critical range (30 to 100) and ranked iron as the dominant contaminant, followed by zinc and copper. The present study's repeated monitoring design instead shows the dominant HPI contaminant shifting between episodes, chromium in the 2021 baseline and nickel in the post-monsoon 2022 peak, with iron the dominant component in only one of eleven critical site-period observations despite its comparatively high absolute concentrations. This discrepancy with Nayak et al. [21] is itself informative, since a single-round snapshot of the kind used in that study would only capture whichever metal happened to dominate at that particular sampling date, not the full episodic pattern. The repeated monitoring design further shows that HPI values exceeded the critical threshold of 100 at all sites during 2021 and, most sharply, in the post-monsoon 2022 period, before falling below 30 from 2023 onward. A single-round HPI assessment, of the kind used in earlier studies of this area, can therefore substantially under- or over-represent both the magnitude and the identity of the underlying pollution pattern depending on when the snapshot falls relative to episodic trace-metal events. This is where repeated monitoring adds most value over single-campaign assessments for metals, even where major-ion water quality appears stable throughout.

A broader comparison with hydrochemical studies of other waste-impacted aquifers is also instructive. Huang et al. [39], using multivariate hydrochemical analysis to distinguish water-rock interaction from contamination-related processes in groundwater affected by a mining tailings pond in northwest China, could separate genuine contamination signatures from background geochemical evolution only with the support of spatial gradients, multivariate ion ratios and, where available, isotopic or mineralogical evidence. The site-characterisation gaps already noted here (well-construction data, background wells; Section 4.4) mean an equivalent separation cannot yet be made with confidence for the Dehradun industrial and MSW-associated sites, despite the broadly similar underlying question; this comparison illustrates the kind of evidence base needed to move the hypotheses proposed in Section 4.1 toward confirmed source attribution. A municipal/industrial pressure-zone setting such as this one also differs from a mining-tailings setting in loading chemistry and history, so direct quantitative comparison of thresholds between the two studies is not attempted here.

4.4. Limitations

Several limitations of this study should be acknowledged. First, the analysis relies on secondary monitoring data compiled by the Uttarakhand State Pollution Control Board. Direct access to laboratory QA/QC records such as blanks, duplicates, certified reference materials, sample containers and preservatives used, and holding times was not available. Lowest Detection Limit values for most analysed parameters were subsequently obtained from the source laboratory's own periodic monitoring reports (Supplementary Table S5), though a matching record could not be located for the four organochlorine pesticides screened in this study, and the specific analytical instruments employed were documented only at the level of general laboratory equipment rather than per parameter. Data quality was otherwise assessed indirectly through internal consistency checks, which identified and flagged one likely transcription error in the electrical conductivity record. A further, more substantial data-quality concern affects six observations (L2, L3 and L4 in October 2021 and L1, L2 and L4 in Pre-Monsoon May 2023), in which the reported sulphate concentration exceeds the reported total dissolved solids for the same sample—a chemically implausible result, since TDS should include sulphate among its constituent ions. Four of these six observations also rank among the four largest-magnitude ionic charge-balance errors in the full 40-observation dataset (-43% to -62%; Section 3.5), confirming that these six observations are the most severe and most specifically identifiable analytical problem in the dataset. All six values were checked against the original State Pollution Control Board laboratory reports and are not transcription errors introduced during compilation; they most plausibly reflect analytical interference or a reporting artefact at the source laboratory, though without access to the original raw analytical traces this cannot be resolved further. However, the charge-balance results are not confined to these six observations: only 22 of 40 (55%) fall within the conventional $\pm 10\%$ acceptance band and 26 of 40 (65%) within $\pm 15\%$ (Section 3.5), indicating a wider analytical uncertainty across the major-ion dataset as a whole. All hydrochemical-facies, charge-balance and irrigation-index interpretations are therefore qualified accordingly: most severely for the six flagged observations specifically (Sections 3.5 and 3.8, and the conclusions), and more generally, with appropriate caution, for the remaining 34 observations given this broader acceptance rate. Second, the five monitoring wells represent two specific anthropogenic pressure zones within the Selaqui-Sisambada area rather than a dense areal network across the wider Doon Valley aquifer, so spatial interpretation should be read at the scale of these pressure zones rather than extrapolated to the aquifer as a whole. Relatedly, site classification was limited to broad industrial-versus-landfill categories without a GIS-based land-use/land-cover analysis or a documented inventory of specific pollution sources (enterprise types, landfill operational history, leachate collection infrastructure) around each well; such an analysis, of the kind used to relate hydrochemistry to land-use structure elsewhere [40], would strengthen future spatial interpretation at these sites. Well-construction details—depth, screened interval, static water level and local groundwater-flow direction—were not available for any of the five wells, nor was background (upgradient or otherwise unimpacted) groundwater chemistry sampled for comparison. As a result, the alkalinity, iron and other chemical contrasts reported between the industrial and MSW-associated site groups (Section 4.1) cannot be attributed to leachate or industrial-discharge influence with confidence from this dataset alone; they are equally consistent with differences in local lithology, residence time or natural carbonate dissolution between the two groups, and are reported as hypotheses rather than confirmed source attributions. Well-construction records and at least one unimpacted background well would be needed to test these hypotheses directly in future monitoring rounds. Third, sampling frequency varied across the study period, from annual in 2021 to semi-annual in 2022 to 2024 and a single round in 2025; a robustness

check restricted to the continuous 2022–2024 window confirmed that this irregularity did not change the conclusion for most reported pooled temporal trends, but the full-period pH and sulphate trends specifically are sensitive to the inclusion of the 2021 baseline and appear driven mainly by recovery from it (Section 3.3). Because 2021 and 2025 were each represented by a single sampling round, seasonal and inter-annual effects cannot be fully separated for those two years specifically, and the eight-round design provides reliable seasonal resolution only for 2022 to 2024. Fourth, a high proportion of non-detect values for several trace metals limited the reliability of pairwise correlation estimates for these parameters, and correlations based on very small numbers of co-occurring non-zero observations were excluded from interpretation rather than reported at face value. Relatedly, the zero-substitution convention adopted for below-detection-limit values, while standard practice for a screening-level assessment of this kind, is a simplification relative to formal censored-data methods such as Kaplan–Meier or regression-on-order-statistics estimators. A sensitivity check (Sections 2.3, 3.6 and 3.7) substituting half of the source laboratory's own documented detection limit for each metal (copper 0.03, nickel 0.1, chromium 0.06 and zinc 0.01 mg/L; Supplementary Table S5) for every zero reading in that metal shows the effect is substantial for both indices: all 29 site-periods classified "low" under zero-substitution move directly to the "critical" band under this alternative convention (HPI 152.9–178.8), the human health hazard index for children exceeds 1 in all 30 pre-monsoon 2022 and 2023–2025 site-period observations, and the adult hazard index also exceeds 1 in 10 of these 30. Because these results rest on the laboratory's own documented detection limits, they indicate that the apparent improvement in heavy metal water quality and health risk from 2023 onward, as reported under the standard zero-substitution convention, may not be robust. They remain an assumption-dependent scenario rather than a confirmed water-quality status, since the true concentration of each non-detect reading lies somewhere between zero and the detection limit and is not known. The non-detect reporting convention for these four metals is therefore a materially consequential source of uncertainty for the post-2021 conclusions of this manuscript, and future monitoring rounds should report quantified low-level trace-metal concentrations wherever the analytical method allows. It should also be noted that several of the documented detection limits are higher than the corresponding BIS IS:10500 acceptable limits (nickel 0.1 against 0.02 mg/L, lead 0.1 against 0.01 mg/L, cadmium 0.02 against 0.003 mg/L and chromium 0.06 against 0.05 mg/L), so a below-detection reading for these metals cannot by itself demonstrate compliance with the drinking-water standard. Detection limits were documented only from the April 2022 round onward, so the consistency of reporting limits between the October 2021 baseline and the later rounds could not be verified. Fifth, dissolved iron was measured without a paired filtered and unfiltered comparison or in situ redox potential, which constrains mechanistic interpretation of the iron mobilisation processes discussed above. Finally, no microbiological parameters were available despite their relevance to a drinking-water context. Continued monitoring that addresses these points, in particular higher-frequency sampling during the post-monsoon period when metal concentrations were highest and redox and speciation measurements for iron, would strengthen future assessments of this aquifer system. Two further limitations concern the human health risk assessment specifically. Chromium speciation (Cr(III) versus Cr(VI)) was not available, so the 2021 hazard index result rests on a conservative worst-case assumption that should be confirmed against laboratory records before being treated as a firm finding. The exposure factors used (ingestion rate, body weight, exposure duration) are also standard international defaults rather than measurements specific to this population, the usual approach in the absence of local exposure survey data, but this should be borne in mind when interpreting the absolute hazard-index values.

5. Conclusions

This study combined five years (2021–2025) of secondary monitoring data across eight sampling rounds with major-ion and trace-metal indexing to assess groundwater quality across two specific industrial and municipal solid waste landfill pressure zones in peri-urban Dehradun, rather than across the wider Doon Valley aquifer. Major-ion chemistry was generally favourable throughout the study period, with a predominantly Ca-HCO_3 hydrochemical facies at the individual-sample level (Section 3.5) and a weighted arithmetic Water Quality Index classifying all site-period combinations as excellent or good. Statistically significant declining trends in TDS, sulphate and sodium, alongside a rising trend in pH, indicate an overall improvement in major-ion water quality between 2021 and 2025, a pattern that remained statistically significant after adjustment for between-site differences in mean concentration; this adjustment, however, does not by itself address temporal autocorrelation within a well or dependence among sites sampled in the same campaign, so the significance levels should still be read with some caution (Section 2.3). A sensitivity check restricted to the continuous 2022–2024 window supported the TDS, sodium and chloride trends, but not the pH and sulphate trends specifically, which appear driven mainly by recovery from the 2021 baseline (Section 3.3).

Against this generally favourable background, a complementary Heavy Metal Pollution Index revealed a sharply different pattern. All five sites experienced at least one period of critical Heavy Metal Pollution Index values, driven by chromium in 2021 and by nickel in the post-monsoon 2022 round rather than by iron, before returning to low values from 2023 onward under the zero-substitution convention used for below-detection-limit copper, nickel, chromium and zinc readings; a sensitivity check substituting half of the laboratory's own documented detection limit for each of these four metals reclassifies all of these low-value site-periods, including those from 2023 onward, into the critical band instead, and raises the child hazard index above 1 in every pre-monsoon 2022 and 2023–2025 site-period (Sections 3.6, 3.7 and 4.4). The human health risk assessment provides a complementary risk-based perspective on the same 2021 window. Using the current USEPA reference dose for hexavalent chromium as an upper-bound screening assumption, the hazard index for combined metal ingestion reached 7.93–10.06 in adults and 18.49–23.46 in children at all five sites in 2021, falling to 0.016–0.071 under the alternative trivalent-chromium assumption (Section 3.7); and a screening-level incremental lifetime cancer risk estimated for the 2021 chromium detections exceeded USEPA's upper acceptable-risk bound under a 30-year bounding exposure scenario, though it falls within the USEPA risk-management range under a shorter, one-year bounding scenario, neither of which is an exposure duration established by the single-round detection itself. This episodic behaviour was not captured by the major-ion WQI alone and would also have been missed by a single-round assessment of the kind used in earlier studies of this area, which is a strong practical argument for reporting major-ion and trace-metal indices separately and for sustaining repeated monitoring rather than relying on single campaigns. Arsenic, mercury, lead, cadmium and four screened organochlorine pesticides remained undetected throughout, indicating no detected contamination by these priority pollutants at any site or time point, although for lead and cadmium the laboratory detection limits exceed the BIS acceptable limits (Section 4.4).

From a management perspective, the results point to episodic trace-metal enrichment, chromium in the 2021 baseline and nickel in the post-monsoon 2022 round, rather than iron mobilisation alone, as the principal water quality concern at these sites, distinct from the major-ion parameters that dominate routine compliance reporting against BIS IS:10500. Because the low post-2021 index values rest on how readings below the detection limit are treated, the apparent recovery from 2023 onward should be regarded as provisional until

it is confirmed with quantified low-level trace-metal measurements in future monitoring rounds (Section 4.4). Possible contributing factors include changes in wastewater management during the 2020–2021 pandemic period and localised reductive mobilisation, though this study's secondary monitoring data cannot confirm a specific cause. MSW-associated sites showed a consistently stronger bicarbonate signature than the industrial cluster. Because chloride was lower rather than higher at these sites, a pattern not typical of leachate alone, and because direct leachate indicators such as ammonium and dissolved organic carbon were not available in this dataset, this bicarbonate contrast is reported as an open question for future monitoring rather than a confirmed leachate contribution, and deserves continued attention even as major-ion indicators remain favourable. A screening-level estimate suggests the 2021 chromium detections could correspond to a lifetime cancer risk above USEPA's acceptable range under sustained worst-case exposure assumptions. This argues for prioritising confirmatory chromium and nickel speciation sampling, not only iron redox and speciation measurements, in future monitoring at these sites, alongside a consistent post-monsoon sampling frequency.

Supplementary Materials: The following supporting information can be downloaded at: https://www.mdpi.com/article/10.3390/environments13100559/s1. Table S1: Site- and period-level Water Quality Index (WQI) values underlying Table 2 (n = 40); Table S2: Site-, period- and receptor-level human health risk assessment values (hazard index and metal-specific hazard quotients) underlying Table 3 (n = 80); Table S3: Site- and period-level Heavy Metal Pollution Index (HPI) values underlying Table 2 (n = 40); Table S4: Site- and period-level ionic charge-balance error (CBE%) values underlying Section 3.5 (n = 40); Table S5: Full inventory of the 33 measured parameters, with units, parameter group, analytical method and Lowest Detection Limit (Section 2.2).

Author Contributions: Conceptualisation, A.B., T.M. and D.B.; methodology, A.B., T.M. and D.B.; software, A.B., D.B.; validation, A.B., T.M. and D.B.; formal analysis, A.B., T.M. and D.B.; investigation, A.B., T.M. and D.B.; resources, A.B., T.M. and D.B.; data curation, A.B.; writing—original draft preparation, A.B., T.M. and D.B.; writing—review and editing, A.B., T.M. and D.B.; visualisation, A.B., T.M. and D.B.; supervision, T.M. and D.B. All authors have read and agreed to the published version of the manuscript.

Funding: Supported by the University of Debrecen Program for Scientific Publication.

Institutional Review Board Statement: Not applicable.

Informed Consent Statement: Not applicable.

Data Availability Statement: The data analysed in this study were obtained from the Uttarakhand State Pollution Control Board and are available from the corresponding author upon reasonable request, subject to permission from the data-providing agency. The Python analysis script and full model outputs generated for this study, including an automated check of every reported statistic against the dataset, are available from the corresponding author upon reasonable request.

Acknowledgments: Not applicable.

Conflicts of Interest: The authors declare no conflicts of interest.

Abbreviations

The following abbreviations are used in this manuscript:

AAS	Atomic Absorption Spectrophotometry
AT	Averaging Time
BDL/ND	Below Detection Limit/Not Detected
BIS	Bureau of Indian Standards
BOD	Biochemical Oxygen Demand
BW	Body Weight

CBE	Charge-Balance Error
CDI	Chronic Daily Intake
COD	Chemical Oxygen Demand
CSF	Cancer Slope Factor
CV	Coefficient of Variation
EC	Electrical Conductivity
ED	Exposure Duration
EF	Exposure Frequency
FAO	Food and Agriculture Organization of the United Nations
HI	Hazard Index
HPI	Heavy Metal Pollution Index
HQ	Hazard Quotient
ILCR	Incremental Lifetime Cancer Risk
IR	Ingestion Rate
IRIS	Integrated Risk Information System (USEPA)
IS	Indian Standard
KR	Kelly's Ratio
LADD	Lifetime-Averaged Daily Dose
LOD/LOQ	Limit of Detection/Limit of Quantification
MH	Magnesium Hazard
MSW	Municipal Solid Waste
%Na	Percent Sodium
OLS	Ordinary Least Squares
PC1, PC2	First and Second Principal Components
PCA	Principal Component Analysis
PI	Permeability Index (Doneen)
QA/QC	Quality Assurance/Quality Control
RfD	Reference Dose
RSC	Residual Sodium Carbonate
SAR	Sodium Adsorption Ratio
SD	Standard Deviation
TDS	Total Dissolved Solids
TKN	Total Kjeldahl Nitrogen
UPCB	Uttarakhand State Pollution Control Board
USEPA	United States Environmental Protection Agency
USSL	United States Salinity Laboratory
UV-VIS	Ultraviolet-Visible (spectrophotometry)
WQI	Water Quality Index

References

1. Gao, Y.; Qian, H.; Ren, W.; Wang, H.; Liu, F.; Yang, F. Hydrogeochemical characterization and quality assessment of groundwater based on integrated-weight water quality index in a concentrated urban area. *J. Clean. Prod.* **2020**, *260*, 121006. [CrossRef]
2. Jasechko, S.; Perrone, D.; Befus, K.M.; Cardenas, M.B.; Ferguson, G.; Gleeson, T.; Luijendijk, E.; McDonnell, J.J.; Taylor, R.G.; Wada, Y.; et al. Global aquifers dominated by fossil groundwaters but wells vulnerable to modern contamination. *Nat. Geosci.* **2017**, *10*, 425–429. [CrossRef]
3. Aeschbach-Hertig, W.; Gleeson, T. Regional strategies for the accelerating global problem of groundwater depletion. *Nat. Geosci.* **2012**, *5*, 853–861. [CrossRef]
4. Haque, M.M.; Rahman, A.; Hagare, D.; Kibria, G. Probabilistic Water Demand Forecasting Using Projected Climatic Data for Blue Mountains Water Supply System in Australia. *Water Resour. Manag.* **2014**, *28*, 1959–1971. [CrossRef]
5. Pant, M.; Singh, J. Computing Water Quality Deterioration Attributed to Anthropogenic Impacts in Dehradun—A Lower Himalayan Region of India. *Environ. Qual. Manag.* **2026**, *35*, e70289. [CrossRef]
6. Alam, A.; Kumar, A.; Singh, A. A GIS approach for groundwater quality evaluation with entropy method and fluoride exposure with health risk assessment. *Environ. Geochem. Health* **2024**, *46*, 47. [CrossRef]

7. Mishra, V.; Dangar, S.; Tiwari, V.M.; Lall, U.; Wada, Y. Summer Monsoon Drying Accelerates India's Groundwater Depletion Under Climate Change. *Earth's Future* **2024**, *12*, e2024EF004516. [CrossRef]
8. Siebert, S.; Burke, J.; Faures, J.M.; Frenken, K.; Hoogeveen, J.; Döll, P.; Portmann, F.T. Groundwater use for irrigation—A global inventory. *Hydrol. Earth Syst. Sci.* **2010**, *14*, 1863–1880. [CrossRef]
9. Singh, A.K. Water Security—A Reality Check. *J. Indian Soc. Soil Sci.* **2018**, *66*, 179–191.
10. Singh, C.K.; Dey, M.K. A Critical Review of India's Latest Groundwater Policy: Impacts on Groundwater Resource Planning and Management. *J. Landsc. Ecol.* **2024**, *17*, 39–59. [CrossRef]
11. Kamboj, V.; Bahukhandi, K.D.; Bisht, A.; Kamboj, N.; Sharma, I.; Semwal, M.P. Groundwater stability and health risk assessment associated with nitrate and fluoride in adjacent areas of Dehradun industrial area, India. *Int. J. Environ. Anal. Chem.* **2025**, *105*, 8950–8965. [CrossRef]
12. Kumar, P.; Thakur, P.K.; Bansod, B.K.S.; Debnath, S.K. Groundwater: A regional resource and a regional governance. *Environ. Dev. Sustain.* **2018**, *20*, 1133–1151. [CrossRef]
13. Kumar, R.; Chauhan, A.; Rawat, L. Physico-Chemical Analysis of Surface and Ground Water in Selected Sites of Dehradun, Uttarakhand, India. *J. Environ. Anal. Toxicol.* **2017**, *7*, 1000420. [CrossRef]
14. Adimalla, N.; Qian, H. Groundwater quality evaluation using water quality index (WQI) for drinking purposes and human health risk (HHR) assessment in an agricultural region of Nanganur, south India. *Ecotoxicol. Environ. Saf.* **2019**, *176*, 153–161. [CrossRef]
15. Raheja, H.; Goel, A.; Pal, M. Assessment of groundwater quality and human health risk from nitrate contamination using a multivariate statistical analysis. *J. Water Health* **2024**, *22*, 350–366. [CrossRef]
16. Kapoor, A.; Anand, M. *Addressing Groundwater Depletion Crisis in India: Institutionalizing Rights and Technological Innovations*; EAC-PM Working Paper Series; Economic Advisory Council to the Prime Minister: New Delhi, India, 2024.
17. Ratandeep; Dharmani, A.B.; Verma, M.; Rani, S.; Narang, A.; Singh, M.R.; Saya, L.; Hooda, S. Unravelling groundwater contamination and health-related implications in semi-arid and cold regions of India. *J. Contam. Hydrol.* **2024**, *261*, 104303. [CrossRef]
18. Pundir, S.; Kandari, V.; Singh, P.; Singh, R.; Siddique, M.A. Assessment of groundwater quality of Dehradun Valley, Uttarakhand, India, for drinking purposes using multivariate statistical techniques. *Environ. Dev. Sustain.* **2022**, *26*, 1749–1779. [CrossRef]
19. Central Ground Water Board (CGWB). Available online: https://cgwb.gov.in/ (accessed on 22 September 2026).
20. Dudeja, D.; Bartarya, S.K.; Biyani, A.K. Hydrochemical and water quality assessment of groundwater in Doon Valley of Outer Himalaya, Uttarakhand, India. *Environ. Monit. Assess.* **2011**, *181*, 183–204. [CrossRef]
21. Nayak, A.; Matta, G.; Uniyal, D.P.; Kumar, A.; Kumar, P.; Pant, G. Assessment of potentially toxic elements in groundwater through interpolation, pollution indices, and chemometric techniques in Dehradun in Uttarakhand State. *Environ. Sci. Pollut. Res.* **2023**, *31*, 36241–36263. [CrossRef]
22. Pandey, K.; Gandhi, F.; Kumar, S.; Roy, C.; Anand, V.; Milentijevic, N.; Pantelic, M.; Dolinaj, D. Regional Variability and Spatio-Temporal Dynamics of Groundwater Quality in the Western Himalayas: An Integrated WQI and Hydrochemical Assessment. *Water* **2026**, *18*, 1602. [CrossRef]
23. USEPA Region III. *Regional Technical Guidance Manual, Risk Assessment, Interim Final*; Hazardous Waste Management Division, Office of Superfund Programs, U.S. Environmental Protection Agency, Region 3: Philadelphia, PA, USA, 1991.
24. Brown, R.M.; McClelland, N.I.; Deininger, R.A.; O'Connor, M.F. A water quality index—Crashing the psychological barrier. In *Indicators of Environmental Quality*; Springer: New York, NY, USA, 1972; pp. 173–182. [CrossRef]
25. *IS 10500:2012*; Drinking Water—Specification (Second Revision). Bureau of Indian Standards: New Delhi, India, 2012.
26. Mohan, S.V.; Nithila, P.; Reddy, S.J. Estimation of heavy metals in drinking water and development of heavy metal pollution index. *J. Environ. Sci. Health A* **1996**, *31*, 283–289. [CrossRef]
27. USEPA. *Risk Assessment Guidance for Superfund, Volume I: Human Health Evaluation Manual (Part A)*; EPA/540/1-89/002; Office of Emergency and Remedial Response: Washington, DC, USA, 1989.
28. USEPA. *Risk Assessment Guidance for Superfund, Volume I: Human Health Evaluation Manual (Part E, Supplemental Guidance for Dermal Risk Assessment)*; EPA/540/R/99/005; Office of Superfund Remediation and Technology Innovation: Washington, DC, USA, 2004.
29. Kelly, W.P. Use of saline irrigation water. *Soil Sci.* **1963**, *95*, 385–391. [CrossRef]
30. Doneen, L.D. *Notes on Water Quality in Agriculture*; Water Science and Engineering Paper 4001; Department of Water Science and Engineering, University of California: Davis, CA, USA, 1964.
31. USSL Staff. *Diagnosis and Improvement of Saline and Alkali Soils*; USDA Agriculture Handbook No. 60; United States Salinity Laboratory: Washington, DC, USA, 1954.
32. World Health Organization (WHO). *Guidelines for Drinking-Water Quality*, 4th ed.; WHO: Geneva, Switzerland, 2011.
33. USEPA. *IRIS Toxicological Review of Hexavalent Chromium [CASRN 18540-29-9] (Final Report)*; EPA/635/R-24/164Fa; Integrated Risk Information System, National Center for Environmental Assessment, Office of Research and Development: Washington, DC, USA, 2024.

34. Aponte, H.; Meli, P.; Butler, B.; Paolini, J.; Matus, F.; Merino, C.; Cornejo, P.; Kuzyakov, Y. Meta-analysis of heavy metal effects on soil enzyme activities. *Sci. Total Environ.* **2020**, *737*, 139744. [CrossRef]
35. Saaltink, R.M.; Dekker, S.C.; Eppinga, M.B.; Griffioen, J.; Wassen, M.J. Plant-specific effects of iron-toxicity in wetlands. *Plant Soil* **2017**, *416*, 83–96. [CrossRef]
36. Sharma, R.K.; Cox, M.S.; Oglesby, C.; Dhillon, J.S. Revisiting the role of sulfur in crop production: A narrative review. *J. Agric. Food Res.* **2024**, *15*, 101013. [CrossRef]
37. Giller, K.E.; Witter, E.; McGrath, S.P. Toxicity of heavy metals to microorganisms and microbial processes in agricultural soils: A review. *Soil Biol. Biochem.* **1998**, *30*, 1389–1414. [CrossRef]
38. Ayers, R.S.; Westcot, D.W. *Water Quality for Agriculture*; FAO Irrigation and Drainage Paper 29, Rev. 1; Food and Agriculture Organization of the United Nations: Rome, Italy, 1985.
39. Huang, X.; Deng, H.; Zheng, C.; Cao, G. Hydrogeochemical signatures and evolution of groundwater impacted by the Bayan Obo tailing pond in northwest China. *Sci. Total Environ.* **2016**, *543*, 357–372. [CrossRef]
40. Biedunkova, O.; Kuznietsov, P.; Tsos, O.; Karaim, O. Hydrochemical Typology of Natural Lakes in the Polissia Region Based on Self-Organizing Maps: Implications for Sustainable Water Resources Management. *Water* **2026**, *18*, 926. [CrossRef]

Disclaimer/Publisher's Note: The statements, opinions and data contained in all publications are solely those of the individual author(s) and contributor(s) and not of MDPI and/or the editor(s). MDPI and/or the editor(s) disclaim responsibility for any injury to people or property resulting from any ideas, methods, instructions or products referred to in the content.